Nucleic Acids Research, 2026, **54**, gkag381
https://doi.org/10.1093/nar/gkag381
RNA and RNA-protein complexes

OXFORD

ADAR1 and ADAR2 associate with the RNA exosome and modulate RNA stability

Dragana Vukić[1,†], Qiupei Du[1,2,†], Anna Cherian[1,2], Damiano Amoruso[1,2], Květoslava Brožinová[1], Ludivine Wacheul[3], Valentina Lacovich[1], Christiane Zorbas[3], Leena Yadav[4], Jiří Sedmík[1,5], Salla Keskitalo[4], Khadija Hajji[1], Stanislav Stejskal[1], Markku Varjosalo[4,6], Denis L.J. Lafontaine[3], Liam P. Keegan[1], Mary A. O'Connell[1,*]

[1]Central European Institute for Technology at Masaryk University (CEITEC MU), Building E35, Kamenice 735/5, 625 00 Brno, Czech Republic
[2]National Centre for Biomolecular Research, Faculty of Science, Masaryk University, Kamenice 5, 625 00 Brno, Czech Republic
[3]RNA Molecular Biology, Fonds de la Recherche Scientifique (F.R.S./FNRS), Université libre de Bruxelles (ULB), Biopark campus, B-6041 Gosselies, Belgium
[4]Institute of Biotechnology, HiLIFE Helsinki Institute of Life Science, University of Helsinki, Viikinkaari 1, 00790 Helsinki, Finland
[5]Present address: Department of Histology and Embryology, Faculty of Medicine, Masaryk University, Kamenice 3, 625 00 Brno, Czech Republic
[6]Institute of Biotechnology, HiLIFE Helsinki Institute of Life Science & Faculty of Medicine, University of Helsinki, Haartmaninkatu 8, 00290 Helsinki, Finland

*To whom correspondence should be addressed. Email: mary.oconnell@ceitec.muni.cz
† The first two authors should be regarded as Joint First Authors.

Abstract

The adenosine deaminase acting on RNA (ADAR) enzymes deaminate adenosine to inosine in double-stranded (ds)RNA. Mammals express two catalytically active enzymes: ADAR1, which is ubiquitously expressed and essential for innate immune homeostasis, and ADAR2, which is enriched in the brain and vascular system. Here, we investigate the ADAR2 interactome and uncover a shared interaction network with ADAR1, including multiple components of the RNA exosome complex, a multi-subunit RNase involved in RNA processing, turnover, and surveillance. The interactions between ADARs and RNA exosome components are nuclear, and resistance to RNase A treatment implies their close proximity. We validated these interactions by immunoprecipitation of both endogenous and epitope-tagged ADAR proteins in multiple cell lines and mapped the interaction interfaces to their dsRNA-binding domains. Exploiting an MS2–MCP tethering system, we show that recruitment of ADAR1 or ADAR2 to the 3′ UTR of a reporter transcript decreases its stability. This decrease in RNA levels was reversed when EXOSC3 was depleted, demonstrating that this destabilizing effect of ADARs on RNA is via the RNA exosome complex. Finally, knockdown of ADARs perturbs rRNA processing, a canonical function of the nuclear exosome, demonstrating a cellular consequence of disrupting ADAR–exosome interactions.

Graphical abstract

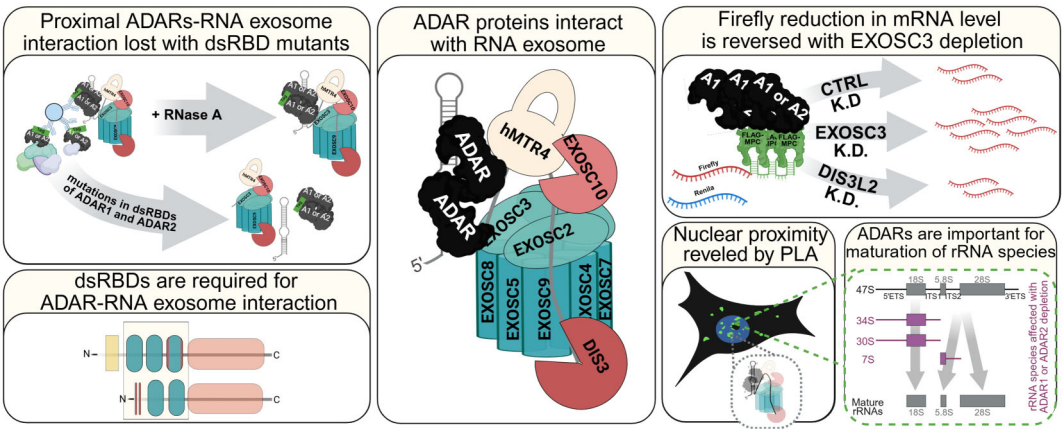

Received: January 5, 2026. **Revised:** March 27, 2026. **Accepted:** April 7, 2026

Introduction

Adenosine-to-inosine (A-to-I) RNA editing is one of the most widespread RNA modifications present in mammals and can have a profound impact on the transcriptome [1]. It is catalyzed by adenosine deaminases acting on RNA (ADARs) enzymes, which deaminate adenosine within double-stranded (ds)RNA (for review [2]). A major source of endogenous dsRNA substrates for ADARs arises from adjacent Alu elements that are inserted in inverted orientations within introns or 3′ UTRs of human transcripts and form dsRNA hairpins (for review [3]). When this dsRNA is unedited, it can activate cytoplasmic dsRNA sensors, which recognize these structures as "non-self" RNA (for review [4]). ADAR1 is primarily responsible for editing dsRNA duplexes formed by repetitive elements, and its deletion or inactivation triggers an innate immune response [4].

ADAR1 exists as two isoforms: ADAR1p110, which is constitutively expressed and predominantly nuclear, and ADAR1p150, which is interferon (IFN)-inducible [5] and mainly cytoplasmic, although both isoforms can shuttle between nucleus and cytoplasm. Its nucleocytoplasmic distribution of ADAR1 is multi-determinant and includes an N-terminal export signal and dsRNA-binding domain-dependent effects on nuclear accumulation/shuttling [6]. Two signals allow ADAR1 to maintain a dynamic balance of intracellular distribution: nuclear localization signal (NLS) and nuclear export signal (NES). The NLS is atypical and overlaps with the third dsRNA-binding domain (dsRBD III) [6, 7]. This NLS functions as an "RNA-sensing switch" because dsRNA binding to the dsRBD sterically hinders the interaction with transportin 1 (Trn1), thereby inhibiting nuclear import [7, 8]. The NES is a leucine-rich signal located in the N-terminal region unique to the ADAR1p150 isoform [6, 7, 9].

The second catalytically active enzyme, ADAR2, is less ubiquitously expressed, being enriched in neural and vascular tissues, and is mainly localized in the nucleus (for review [10]). The ADAR2 NLS is located in its N-terminal region and does not contain a region homologous to the dsRBD-overlapping NLS of ADAR1, it consists of two highly conserved basic clusters within residues 48–72 [11–13]. The ADAR2 is typically nuclear and has been reported to accumulate in the nucleolus [11, 14]. In addition, both ADAR1p110 and ADAR2 are prominently enriched in the nucleolus, where their sequestration is thought to limit excessive activity by restricting access to nucleoplasmic substrates [14, 15]. ADAR2 is primarily responsible for site-specific RNA editing events. When this occurs within coding regions, inosine is interpreted as guanosine by the translation machinery, thereby altering the encoded amino acid and potentially having profound consequences on protein function [16]. Many of the transcripts that undergo site-specific RNA editing are expressed in the nervous and vascular systems. The frequency of site-specific editing can be very efficient; for example the *GRIA2* pre-mRNA is edited to 100% at the Q/R site [17], while edited adenosines within repetitive elements are typically numerous but individual adenosines are each edited at lower frequencies [18].

Both ADAR1 and ADAR2 share a conserved domain architecture consisting of a C-terminal deaminase domain and multiple dsRBDs, with ADAR1 having additional N-terminal domains: Zα and Zβ (for review [19]). These modular features allow ADARs to engage with structured RNAs and to interact with proteins that can modulate ADAR activity, localization, and substrate specificity. Several proteomics studies have defined the ADAR interactomes [20–23], identifying associations with RNA-binding proteins, helicases, and factors involved in RNA processing. In our previous study, we also showed that the two isoforms of ADAR1 have distinct proximal protein networks that rely heavily on dsRNA binding. Moreover, during IFN stimulation, the core interactome remained largely unchanged, whereas newly identified interactors were predominantly regulators of the IFN response [21]. In this study, among the different interactors and proximal proteins identified are subunits of the RNA exosome complex. This interaction between the RNA exosome and ADAR1 had been previously reported through mass spectrometry analyses, but these interactions have not been further studied [20–25].

The RNA exosome is a multi-subunit 3′→5′ exoribonuclease that plays a key role in RNA processing (production of mature ends), turnover (degradation), and surveillance (quality control) in both the nucleus and the cytoplasm (for review [26, 27]). The core exosome consists of a catalytically inert nine-subunit ring that associates with catalytic nucleases, for example EXOSC10 (also known as hRRP6) and hDIS3 in the nucleus (for review [27]). In addition, a set of associated cofactors and adaptors, including the nuclear RNA helicase hMTR4 (SKIV2L2, MTREX), which is a central component of all nuclear adaptors characterized to date, are required for exosome regulation and for the recruitment of specific RNA substrates to the complex [27, 28]. The NEXT (nuclear exosome targeting) complex is an example of an MTR4 adaptor complex that targets non-polyadenylated RNAs arising from spurious transcription events in the surveillance of snoRNA precursors [25, 29, 30], while PAXT targets polyadenylated transcripts [31–33].

Many exosome substrates, including small nucleolar RNAs, cryptic unstable transcripts, precursors of ribosomal RNAs, and RNA:DNA hybrids, contain long or structured dsRNA regions reminiscent of ADAR substrates, raising the possibility that ADARs and the exosome may act, and possibly cooperate, on overlapping RNA populations. ADAR2 can also affect RNA stability by altering local structure or by modulating recognition by decay-promoting RNA-binding proteins [34]. Similarly, ADAR1 has also been linked to RNA stability through interactions with HuR [35] and through editing-dependent effects on Staufen-mediated messenger RNA (mRNA) decay under stress conditions [36]. However, until now a direct mechanistic link between the RNA exosome and ADARs has not been established.

Here, we report the interactome of ADAR2. Our analysis identified multiple subunits of the RNA exosome as ADAR2 interactors, and comparison with published ADAR1 datasets revealed several common components. We validated interactions between ADAR1/ADAR2 and multiple nuclear RNA exosome subunits by co-immunoprecipitation (co-IP) of endogenous proteins across multiple cell lines and of epitope-tagged ADAR proteins. These interactions are nuclear and are resistant to RNase A treatment *in vitro*, indicating that ADARs and exosome components engage in proximal associations. Protein domain mapping assays demonstrated that both the dsRBDs and the NLS of both ADAR proteins are required for interaction with the RNA exosome. To investigate the functional significance of ADAR's interaction with RNA exosome, we deployed an MS2–MCP tethering assay in combination with a series of ADAR deletions. Tethering ADARs to the 3′

UTR of a reporter transcript reduced both luciferase activity and mRNA abundance. This effect was reversed by the knockdown of EXOSC3, a core component of the exosome essential for its function, demonstrating that ADAR-mediated destabilization depends on the RNA exosome. Finally, to assess whether ADAR also contributes to the metabolism of endogenous RNAs, we turned to the nucleolus, where ADAR localizes, since a large fraction of the interactors identified in our analysis are nucleolar proteins and ribosome assembly factors. We first examined its potential role in the formation of the 3′ end of 5.8S rRNA, a classical RNA exosome substrate on which this exoribonuclease complex was originally characterized [37]. We found that ADAR is indeed involved in this process. Moreover, ADAR contributes to additional processing steps, including 5′ ETS maturation, consistent with its interaction with other processing factors. Its depletion also affects other aspects of ribosome biogenesis, notably altering 2′-O-methylation at specific sites, likely reflecting changes in the kinetics of ribosomal subunit assembly.

Materials and methods

Preparation of expression constructs

Full-length human ADAR1 (p110 and p150) and ADAR2 wild-type (WT), catalytically inactive, dsRNA-binding-deficient, and deletion plasmids were generated with Gateway™ recombination and recombined into tetracycline-inducible pTO_HA_StrepIII_GW_FRT expression vector [38]. The dsRNA-binding-deficient ADAR2 mutant encoding K127A and K281A substitutions was generated by site-directed polymerase chain reaction (PCR) mutagenesis. Plasmids for MS2–MCP tethering assays were FLAG epitope-tagged and cloned into pcDNA5/FRT/TO (Invitrogen) vector encoding the MS2 coat protein. MS2 stem-loop sequence was inserted into the 3′ UTR of firefly luciferase in the pmirGLO reporter vector (Promega). All constructs were verified by Sanger sequencing. Detailed cloning strategies, primer sequences, and mutagenesis procedures are provided in the Supplementary data.

Cells and culture conditions

HEK293T (ATCC, CRL-3216) cells were maintained in Minimum Essential Medium (MEM) with Earle's salts (Biosera, #LM-E1141), and HeLa cells (ATCC, CRM-CCL-2), A549 cells (ATCC, CCL-185), and PaTu cells (DSMZ) were cultured in high-glucose DMEM (Biosera, #LM-D1110). Media were supplemented with 10% FBS (Merck, #F7524), 1× non-essential amino acids (Thermo Fisher Scientific, #11140-050), and 1% penicillin–streptomycin (Biosera, #XCA4122). Flp-In™ T-REx™ 293 and T-REx™ HeLa cells (Invitrogen) DMEM low glucose (Biosera, #LM-D1110) supplemented with 10% tetracycline-free FBS (Biosera, #1001T) and 1% penicillin–streptomycin. All cell lines were grown as adherent monolayers at 37°C in 5% CO_2.

Stable cell lines expressing SHN-tagged WT, mutant protein, or deletion constructs of ADAR1 and ADAR2 were generated with the Flp-In™ T-REx™ system and selected with hygromycin. Expression of epitope-tagged proteins was induced with tetracycline, and control cell lines were generated in parallel. Detailed cloning strategies, selection conditions, and cell line validation are provided in the Supplementary data.

Affinity purification of ADAR2 protein complex and LC-MS/MS analysis

Full details regarding the analysis and data evaluation are in Supplementary data. In summary, Flp-In T-REx™ 293 positive cells were expanded and induced for ADAR2 WT-SHN bait expression with 1 μg/ml of doxycycline for 24 h. Strep-tag affinity purification of ADAR2 WT-SHN or GFP-SHN-expressing 293 T-REx cell lines was performed as described in [39] and in Supplementary data. Protein complexes were isolated with Strep-Tactin beads (IBA GmbH) under non-denaturing conditions. Eluted protein complexes were reduced, alkylated, and digested with 5 mM TCEP [Tris(2-carboxyethyl) phosphine], 10 mM iodoacetamide (IAA), and 1 μg trypsin (Promega), respectively. Digested peptides were quenched with trifluoroacetic acid (TFA), desalted with C18 MicroSpin columns (The Nest Group), and vacuum dried. Later, samples were revived in 30 μl HPLC solvent A (0.1% formic acid and 1% acetonitrile in HPLC water). LC-MS analysis was performed on EASY-nLC II reverse-phase HPLC nanoflow system coupled to LTQ Orbitrap XL or Velos Pro Orbitrap Elite hybrid mass spectrometers with the Xcalibur version 2.7.0 (Thermo Fisher Scientific). Data analysis was performed with the Fragpipe analysis platform (version 22.0) with MSFragger (version 4.1) [40, 41] and Philosopher (version 5.1.1) [42] for peptide identification using raw files as an input.

High confidence interactors and protein network visualization

High confidence interactors (HCIs) and protein network visualization. HCIs of ADAR2 were defined as described previously [43] with SAINT filtering [44] with the following cut-offs: BFDR < 0.05, average spectral count >4, fold change >4, and SAINT score >0.9. Proteins were further filtered against the CRAPome database [45]: candidates with <20% frequency in CRAPome were retained, whereas for proteins with >20% CRAPome frequency, a relaxed fold-change cut-off of 2 was applied. Protein interaction networks were generated with STRING v12.0 (physical interaction subnetwork, medium confidence 0.4) [46] and visualized in Cytoscape v3.10.3 [47].

Co-immunoprecipitations

Cells expressing SHN-ADAR constructs were cultured under standard conditions in 100 mm Petri dishes and, where indicated, protein expression was induced with doxycycline (200 ng/ml, Applichem, #A2951) for 24 h. Cells were lysed under non-denaturing conditions [lysis buffer composition: 150 mM NaCl, 50 mM HEPES pH 8.0, 5 mM ethylenediaminetetraacetic acid (EDTA), 0.5% NP-40, 10% glycerol, supplemented with Halt™ Protease Inhibitor Cocktail, EDTA-free (2×, Thermo Fisher, #78439), and 1× Halt™ Phosphatase Inhibitor Cocktail (Thermo Fisher, #78427)] for 30 min. Clarified lysates were subjected to co-IP with anti-HA or Strep-tactin beads, depending on the experiment. For deletion and mutant analyses, co-IPs were performed with either transiently transfected or stable Flp-In™ T-REx™ 293 cell lines expressing SHN-tagged ADAR1 or ADAR2 constructs and processed as described earlier and in Supplementary data. Bead-bound complexes were extensively washed under low- or high-salt conditions, eluted in Laemmli sample buffer, and analyzed by sodium dodecyl sulfate–polyacrylamide gel elec-

trophoresis (SDS–PAGE) and immunoblotting as described below. Input and immunoprecipitated samples were processed in parallel. For RNase sensitivity assays, lysates were treated with RNase A (10 μg/ml; Thermo Fisher, #EN0531) prior to the IP. Where indicated, RNA was extracted from IPed material for downstream analysis. Detailed buffer compositions, protein amounts, bead types, washing conditions, and replicate-specific procedures are provided in the Supplementary data.

Endogenous co-IP experiments were performed in HeLa and HEK293T cells grown to near confluency. Cells were lysed under non-denaturing conditions (lysis buffer: 50 mM Tris–HCl, pH 8.0; 150 mM NaCl; 0.5% NP-40; 1 mM EDTA, pH 8.0; 10% glycerol) in the presence of 2× Halt™ Protease Inhibitor Cocktail, EDTA-free (Thermo Fisher, #78439) and 1× Halt™ Phosphatase Inhibitor Cocktail (Thermo Fisher, #78427), and clarified lysates were pre-cleared with Dynabeads™ Protein G (Thermo Fisher, #10003D). Equal amounts of total protein were incubated overnight with antibodies against the indicated endogenous proteins or with species-matched control IgG (Supplementary Table S4). Immune complexes were captured with Dynabeads™ Protein G (Thermo Fisher, #10003D), washed with wash buffer (200 mM NaCl, 50 mM HEPES pH 8.0, 1 mM EDTA, 0.5% NP-40), eluted in Laemmli sample buffer, and analyzed by SDS–PAGE and immunoblotting as described below. Input samples were processed in parallel. Detailed lysis conditions, antibody amounts, bead volumes, and wash parameters are provided in the Supplementary data.

Immunoblotting of co-IP samples and total cell lysates

Whole-cell lysates were prepared in non-denaturing lysis buffer (50 mM HEPES pH 8.0, 150 mM NaCl, 5 mM EDTA, 0.5% NP-40) supplemented with 1× Halt™ Protease Inhibitor Cocktail, EDTA-free (Thermo Fisher, #78439) and 1× Halt™ Phosphatase Inhibitor Cocktail (Thermo Fisher, #78427), and clarified by centrifugation. Protein concentrations were determined by BCA assay (Pierce™ BCA Protein Assay Kit, #23225). An equal amount of protein or input and bound fractions from co-IP experiments were resolved by SDS–PAGE and transferred to nitrocellulose membranes (VWR, #10600003). Membranes were incubated with primary antibodies overnight at 4°C, followed by an hour incubation with HRP-conjugated secondary antibodies at room temperature. Antibodies used and their dilutions are listed in Supplementary Table S4. Signals were detected with enhanced chemiluminescence (Bio-Rad, #1705061) and imaged with a UVITEC ChemiDoc system. More details are in the Supplementary data. Immunoblot signal intensities were quantified with ImageJ, and band intensities were normalized to the indicated controls.

Immunofluorescence and proximity ligation assay

Cells were grown on glass coverslips, fixed with 4% paraformaldehyde (Thermo Scientific, #J61899), and permeabilized with 0.2% Triton X-100. Immunofluorescence was performed as previously described [21]. The proximity ligation assays (PLA) were performed as previously described [48] with the Duolink® *In Situ* PLA system (Sigma–Aldrich). Primary and secondary antibodies are listed in Supplementary Table S4. Confocal images were acquired with a Zeiss LSM 780 microscope with a 63× oil-immersion objective (NA 1.4). Raw image processing was performed with Fiji/ImageJ [49], and PLA signal quantification with the Particle Analysis plugin in Fiji/ImageJ. Data were obtained from 3–4 independent biological replicates per condition, with variable numbers of nuclei analyzed per replicate. Statistical significance was assessed with Kruskal–Wallis tests followed by Mann–Whitney post-hoc tests with Holm correction against the control condition. More detailed information is available in Supplementary data.

MS2–MCP tethering assay experimental method

HEK293T cells were co-transfected with plasmids encoding MCP-tagged full-length ADAR proteins, deletion mutants, or GFP control, together with the pmirGLO-MS2 stem-loop reporter, with Lipofectamine™ 3000 (Invitrogen, #L3000015) according to the manufacturer's instructions. After 18–20 h, cells were harvested for immunoblotting or lysed in TRIzol for RNA analysis. For knockdown experiments, cells were transfected with 30 nM siRNAs (Eurofins) targeting EXOSC3, DIS3L2, or scrambled control (Supplementary Table S3) with Lipofectamine™ RNAiMAX (Invitrogen, #13778075). Approximately 30 h later, cells were co-transfected with MCP-tagged constructs and the reporter plasmid with Lipofectamine™ 3000. Cells were harvested 18 h after plasmid transfection for immunoblotting and RNA analysis. Immunoblotting was performed as described above, and antibodies are listed in Supplementary Table S4.

Dual-luciferase reporter assay

Firefly and Renilla luciferase activities were measured with Dual-Glo® Luciferase Assay System (Promega, #E2920) according to the manufacturer's instructions. Firefly activity was normalized to Renilla activity within each biological replicate and then to GFP control. Data are presented as mean ± SEM from at least three independent biological replicates per construct.

RNA extraction, cDNA synthesis, and quantitative PCR

Total RNA was extracted with TRIzol reagent (Sigma–Aldrich, #T9424) according to the manufacturer's instructions. Extracted RNA was treated to minimize plasmid-derived DNA contamination as described in Supplementary data (LiCl precipitation and Turbo DNase digestion with subsequent precipitation). Reverse transcription was performed with RevertAid Reverse Transcriptase Kit (Thermo Fisher Scientific, #EP0442) with oligo(dT) primers. Quantitative PCR (qPCR) was performed on a LightCycler® 480 Instrument II (Roche) with SYBR Green chemistry. Reactions contained 10 ng of cDNA and gene-specific primers (listed in Supplementary Table S2). Relative RNA levels were calculated with the comparative Ct method ($2^{-}\Delta\Delta Ct$) and normalized to Renilla luciferase mRNA. Statistical significance was assessed with Welch's ANOVA followed by Games–Howell post-hoc tests against the GFP control in RStudio [50, 51].

Analysis of pre-rRNA processing in ADAR-depleted cells

Pre-rRNA processing of low-molecular-weight species was analyzed by northern blotting. Total RNA (5 μg) was dried and resuspended in acrylamide loading dye (50% v/v for-

mamide, 20 mM EDTA, 0.025% w/v xylene cyanol, 0.025% w/v bromophenol blue). Samples were separated on 8% polyacrylamide/1× TBE gels for 4 h at 350 V. RNA was transferred to nylon membranes (GE Healthcare, RPN203B) by electrotransfer in 0.5× TBE. Membranes were prehybridized for 1 h at 65°C in hybridization buffer (50% v/v formamide, 5× SSPE, 5× Denhardt's, 1% w/v SDS, 200 µg/ml salmon sperm DNA; Roche, 11467140001). Pre-rRNA processing of high-molecular-weight species was analyzed by northern blotting after separation of total RNA in 1.2% formaldehyde/agarose gels, migrated for 16 h at 60 V. A ^{32}P-labeled oligonucleotide probe (LD2079: GGGGCGATTGATCGGCAAGCGACGCTC; or LD1827: CCTCGCCCTCCGGGCTCCGTTAATGATC) was generated with T4 polynucleotide kinase (NEB, M0201S) according to the manufacturer's protocol. Membranes were hybridized with the probe for 1 h at 65°C, followed by overnight incubation at 37°C. After washing in 3× SSC, membranes were exposed to phosphorimaging plates (Fujifilm). Signal quantification was performed with a Fujifilm FLA-7000 phosphorimager and MultiGauge software (Fujifilm).

Analysis of rRNA 2′-O-methylation levels by RiboMeth-seq

RiboMeth-seq was performed as described in [52]. A total of 150 ng of total RNA was used per reaction.

Statistical analysis and visualization of the data

All graphical data visualization in this manuscript was made with RStudio (v. 2022.07.2 + 576 with R v. 4.2.2). Graphical abstract and schemes displayed in some figures was made with BioRender. Relevant statistical tests are indicated.

Results

Overlapping stable ADAR interactomes highlight interactions with the RNA exosome complex and nucleolar proteins involved in ribosome biogenesis

ADAR2, one of the two catalytically active ADAR RNA editing enzymes, is detected across multiple tissues, with peak of expression in neuronal and vascular tissues, and is localized at the subcellular level in the nucleus with nucleolar enrichment (for review [10]). Various editing regulators [53] and a BioID-based proximity-labeling study [20] outlining the protein network in the vicinity of ADAR2 have been previously described. However, proximity-labeling approaches capture spatially proximal proteins and do not distinguish stable ADAR2-containing complexes from transient or indirect associations. In addition, although affinity-purification mass spectrometry (AP-MS) has previously been used to identify candidate ADAR2-associated proteins, these studies were primarily focused on identifying specific regulators of RNA editing activity, such as DHX9 [23], rather than defining a comprehensive, high-confidence ADAR2 interactome.

To systematically define stable ADAR2-associated proteins, we performed strep-tag affinity purification followed by label-free LC-MS/MS (see the "Materials and Methods" section). To accomplish this, we generated doxycycline-inducible Flp-In™ 293 T-REx cells (henceforth referred to as 293 T-REx) expressing ADAR2 with Strep II-HA tags at the N-termini (SHN). Bait recovery was robust (Supplementary Fig. S1A). HCIs were defined with SAINT [44] and CRAPome [45] filtering criteria, as described in the "Materials and methods" section. These filtering steps yielded 107 HCIs of ADAR2 in total out of 601 detected proteins (Supplementary Fig. S1B and Supplementary Table S1). Of these, 31 ribosomal proteins were excluded from comparative analysis because of their small size and highly charged nature, making it quite difficult to know if they are *bona fide* partners or not. However, it is likely that they are true interactors, considering the remarkable diversity of enriched ribosome assembly factors and nucleolar proteins with ADAR2 (Fig. 1C, see all interactors displayed in the center). Cross-referencing the ADAR2 HCI set with BioGRID [54], IntAct [55], and the published ADAR2 BioID dataset [20] recovered 53 previously reported interactors and 23 novel interactors were revealed by our AP-MS analysis (Fig. 1A).

The other catalytically active A-to-I enzyme in human cells is ADAR1. To assess whether the two ADAR proteins share components of their protein complexes, we compared the obtained ADAR2 HCI set with curated ADAR1 interactions from BioGRID and IntAct databases, as well as with the published ADAR1 AP-MS interactome [21]. Note that we compared the ADAR1p110 and ADAR1p150 isoforms separately while combining DDA and DIA as in the original report. Of the 76 ADAR2 interactors, 61 were shared with the combined ADAR1 isoforms' datasets, whereas 15 HCIs were unique to ADAR2 (Fig. 1B). Similar conclusions were reached when the ADAR1 data were stratified by acquisition method (DDA versus DIA; Supplementary Fig. S1C). The substantial overlap is consistent with their shared nuclear localization, dsRNA binding capacity, and roles in RNA editing.

We next constructed a physical protein–protein interaction network of the ADAR2 HCI set with STRING [56] and visualized it in Cytoscape [47], which identified three distinct clusters (Fig. 1C and Supplementary Fig. S1D). In this analysis, node size reflects ADAR2-normalized spectral counts, blue node outlines mark proteins also detected with ADAR1, and node fill distinguishes previously reported from novel ADAR2 interactors. The largest cluster, in the center of display comprises dozen key ribosome biogenesis factors and nucleolar proteins (e.g. NOP2, DDX24, RRP12, etc.). The second cluster (right) contains a mix of proteins, including zinc finger motif proteins and CRD-mediated mRNA stabilization proteins that have the highest spectral counts and are thus the most abundant interactors, and include well-known ADAR interactors, such as ILF2/ILF3, ZFR, and DHX9. Remarkably, a third cluster to the left is formed by multiple subunits of the RNA exosome complex. In total, all nine core exosome components were detected with our approach, of which four subunits of the core—EXOSC2, EXOSC3, EXOSC5, EXOSC8, and the ribonuclease EXOSC10—passed HCI filtering (Supplementary Fig. S1E). Among these ADAR2 HCIs, four subunits—EXOSC2, EXOSC3, EXOSC5, and EXOSC8—have not previously been annotated as ADAR2 interactors. However, these proteins were reported as ADAR1 interactors as indicated by blue node outline, suggesting that both ADAR1 and ADAR2 associate with components of the RNA-turnover machinery. Consistent with this, EXOSC10, the processive exoribonuclease of the RNA exosome, has been repeatedly observed on ADAR-centric interaction maps [20, 21, 22], supporting the notion that the ADARs and RNA exosome interact robustly.

Collectively, these data establish a stable, high-affinity interactome of ADAR2 in 293 T-REx cells that substantially

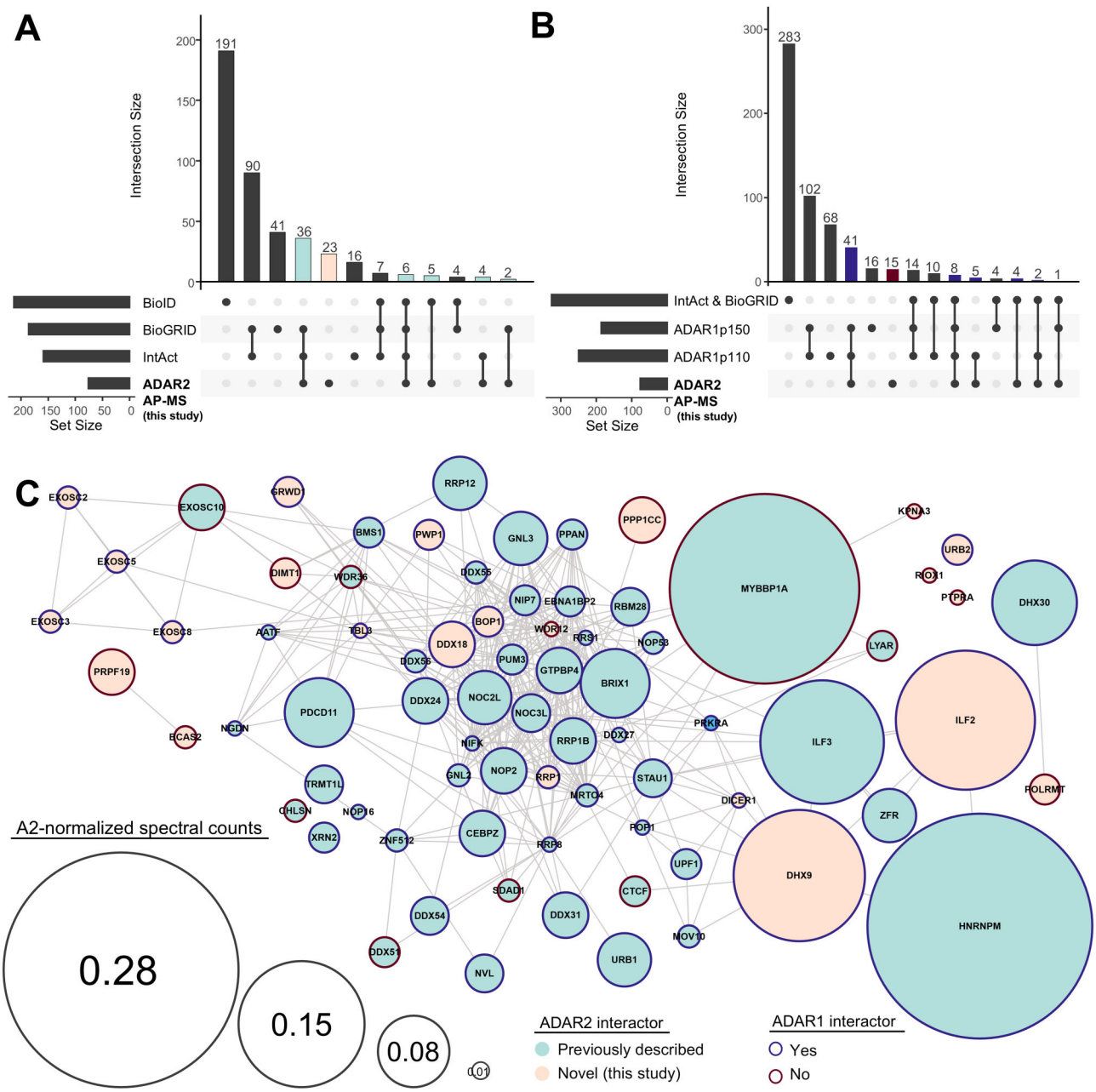

Figure 1. Cross-dataset support for the ADAR2 interactome and network context. (**A**) UpSet plot summarizing overlap of ADAR2 AP-MS HCIs (this study) with reference resources, including two databases (IntAct and BioGRID) and a proximity-labeling dataset (BioID). Bars show the number of proteins in each exact intersection (dot matrix below); mint-colored bars mark intersections that include A2 AP-MS, and light peach bars denote proteins unique to this study. Set sizes are shown as horizontal bars on the left of each plot. (**B**) UpSet plot summarizing overlap of ADAR2 AP-MS HCIs (this study) with published ADAR1 interactomes (p110 and p150 isoforms; DIA/DDA combined) and the database (union of IntAct + BioGRID). Bars show the number of proteins in each exact intersection (dot matrix below); blue bars mark intersections that include A2 AP-MS HCIs, and red bars denote proteins unique to ADAR2 AP-MS. Set sizes are shown as horizontal bars on the left of each plot. (**C**) STRING protein–protein interaction network of ADAR2 HCIs visualized in Cytoscape. Nodes are HCIs, and edges represent the STRING interaction combined score. Node size is proportional to the spectral count for each interactor, normalized to the ADAR2 spectral count. Node fill indicates colors from the UpSet encoding from panel (A): teal = previously described interactor, peach = novel in this study. Node outline colors correspond to the UpSet encoding from panel (B): blue = identified as ADAR1 interactor, red = not described as ADAR1 interactor.

overlaps with the interactome of ADAR1, which is enriched for components of the RNA exosome degradation complex, key ribosome biogenesis components, and nucleolar proteins.

ADAR–exosome interactions withstand RNase A treatment but are eliminated by dsRBD mutations

Next, we validated the interaction between ADARs and the RNA exosome components. Doxycycline-inducible 293 T-REx lines expressing either GFP, ADAR1p110, ADAR1p150, or ADAR2, each having an SHN epitope tag, were treated with doxycycline for 24 h prior to HA epitope tag-mediated co-immunoprecipitation, and interacting partners were identified by immunoblotting. To achieve a comparable signal across the different ADAR baits, the amounts of protein were adjusted. Co-IP of ADAR1p110, ADAR1p150, and ADAR2 precipitated the exosome components EXOSC3, EXOSC8, and EXOSC10, the exosome-associated helicase hMTR4, and known interactors of both ADAR1 and ADAR2: DHX9 [23], ILF2 [20, 57], ILF3 [20, 57], as well as ADAR1 interactor hnRNPC1/2 [21] (Fig. 2 and Supplementary Fig. S2). To test whether the interactions between ADARs and RNA exosome components are bridged by a long RNA molecule, lysates were pre-treated with RNase A for 1 h prior to co-IP (Fig. 2A and Supplementary Fig. S2A and C). Replicate-compiled heatmaps (values normalized to the GFP IP control; replicate number indicated in brackets) showed comparable enrichment of RNase treatment to untreated samples across tested RNA exosome components, with no systematic loss in signal intensity (Fig. 2A, left). Similar to the RNA exosome components, following RNase A digestion and co-IP, previously published interactors of ADARs, including ILF2, ILF3, and DHX9, appear to be largely unaffected. In contrast, interaction of either ADAR1 or ADAR2 with hnRNPC1/C2 was lost, consistent with hnRNPC1/C2 binding to long single-stranded RNA, providing a technical control for RNase digestion efficacy. Representative blots illustrating these interaction patterns are shown (Fig. 2A, right and Supplementary Fig. S2A and C). These data implied that the ADAR–exosome interactions were largely RNase A-resistant, consistent with either protein-protein contacts or bridged via short/structured dsRNA fragments that persisted after RNase A digestion [58] (Supplementary Fig. S2B).

Taking this into consideration, we further tested if dsRNA-binding-deficient forms of ADARs would interact with RNA exosome components or not. Doxycycline-inducible 293 T-REx cells were generated to express individual ADAR1 and ADAR2 dsRNA-binding-deficient mutants [59]. In both ADAR1 and ADAR2, conserved lysine residues within the dsRBDs contact the phosphate backbone of dsRNA, and their substitution disrupts dsRNA binding and catalytic activity [59]. For ADAR1, we employed the previously described EAA substitutions within all three dsRBDs (K→E/A), and for ADAR2, we generated a dsRNA-binding mutant having point substitutions in each dsRBD as described in the "Materials and methods" section. Introducing mutations into the dsRBDs of ADAR1p110 and ADAR1p150 or ADAR2 resulted in a complete loss of interaction of all tested exosome components—EXOSC3, EXOSC8, and EXOSC10—hMTR4, and known ADAR-interacting proteins, as shown in the heatmaps and representative immunoblots (Fig. 2B and Supplementary Fig. S2D and E). This behavior is consistent with previous observations of a complete loss of stable interactions, of changes in the proximal protein network, and of changes in the subcellular localization of ADAR1 dsRNA-binding mutants [21].

Altogether, these results indicate that although ADAR1 and ADAR2 interaction with the RNA exosome components does not depend upon a long RNA molecule, ADAR-dsRNA binding capacity is essential for the formation of these protein interactions.

Reciprocal co-IPs reveal endogenous ADAR–RNA exosome complexes in HeLa and HEK293T cells

To determine whether the interactions observed with the overexpressed ADAR enzymes are detectable at endogenous ADAR expression levels and conserved across different cellular backgrounds, we performed reciprocal co-IPs in two distinct human cell lines: HEK293T and HeLa. First, we co-IPed either endogenous ADAR1 with an antibody that recognizes both the ADAR1p150 and ADAR1p110 isoforms or endogenous ADAR2. The RNA exosome components EXOSC3, EXOSC8, and EXOSC10, the helicase hMTR4, and the known ADAR1 and ADAR2 interactors DHX9, ILF3, and hnRNPC1/C2 were all detected by immunoblotting, confirming interaction (Fig. 3A and Supplementary Fig. S3A). A compiled heatmap of replica experiments with values normalized to the IgG co-IP control, shows that in both cell lines ADAR1 and ADAR2 robustly co-IPed EXOSC10 and hMTR4 with consistent enrichments relative to controls. Interactions with EXOSC3 and EXOSC8 were generally difficult to obtain (Fig. 3A and B). The mean values of EXOSC3 and EXOSC8 were slightly higher for ADAR1, but similar to IgG control for ADAR2. This could be due to the smaller protein sizes of these exosome subunits and their proximity to the strong immunoblot signals from the heavy and light chains of antibodies, which hindered their detection. Another possible explanation is that, although we detected EXOSC3 and EXOSC8 as HCIs, the amount of ADAR proteins interacting with them is lower than that with EXOSC10 and hMTR4.

We also performed the reciprocal co-IPs, where endogenous RNA exosome subunits were co-IPed and bound fraction was analyzed for the presence of endogenous ADAR1 and ADAR2 (Fig. 3B and Supplementary Fig. S3B). As with the ADAR co-IP experiments, a rabbit IgG isotype served as a negative control, and endogenous DHX9 was included as a positive control for ADAR1 interactors. As seen on the heatmap and representative immunoblots, co-IP with RNA helicase hMTR4 and the two exosome components EXOSC10 and EXOSC9 efficiently recovered both isoforms of endogenous ADAR1 and ADAR2 in both cell lines. We also observed strong mutual co-IP among exosome components, validating efficient detection of the protein complex.

Across both cell lines, ADAR1p110 and ADAR2 showed strong and largely comparable enrichments with RNA exosome components. By contrast, the ADAR1p150 isoform was detectable with weaker enrichment, which likely reflects its lower expression under non-IFN conditions and/or a bias toward exosome interactions occurring in the nuclear compartment. Together, these co-IP experiments support a relevant physiological association between endogenous ADAR proteins and RNA exosome components in two different cell lines.

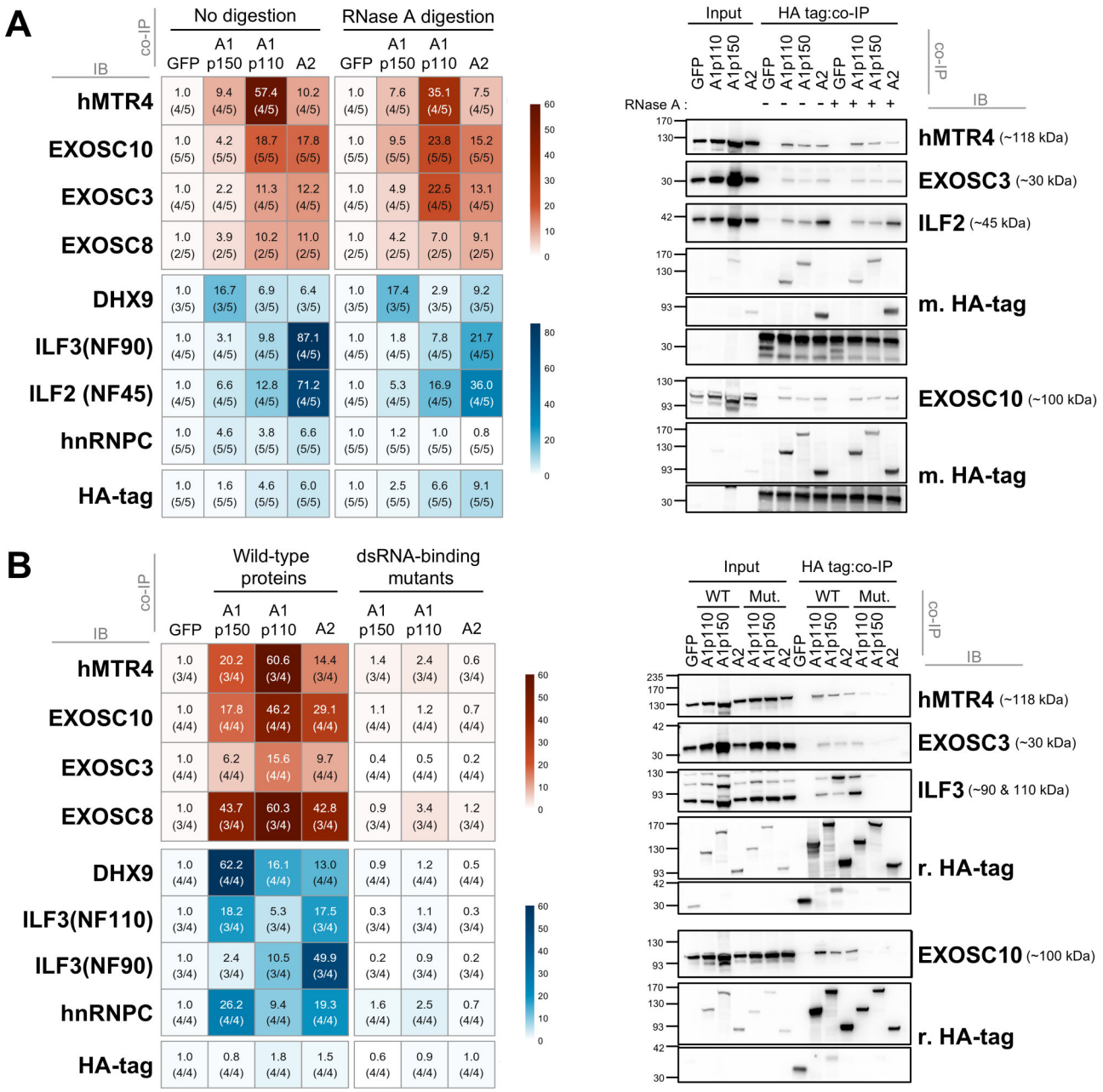

Figure 2. Proximal interactions between ADARs and exosome components depend on ADAR dsRNA-binding. (**A**) An interaction proximity validation with RNase A treatment. Left, heatmaps; right, representative immunoblots. Total lysates were treated with RNase A for 1 h at 4°C (+RNase A) or left untreated, then subjected to 1 h anti-HA co-IP. (**B**) ADAR dsRNA-binding requirement for interaction. As in panel (A), but with WT ADAR1/ADAR2 and dsRNA-binding mutants (Mut.). In both panels, doxycycline-inducible 293 T-REx cells expressing StrepII-HA-ADARs (A1p110, A1p150, and A2) or GFP-StrepII-HA (control) were used. Heatmap tiles show GFP-normalized enrichment of the bound fraction (value printed in the tile); numbers in parentheses indicate detection frequencies across replicates. Palettes: red tiles denote novel interactors; blue tiles denote previously reported ADAR interactors. Inputs = 1% of lysate; bound lanes contain one-half of the eluate. Blots were probed for exosome components and known ADAR partners; HA reports bait recovery (mouse or rabbit anti-HA, as indicated), and the predicted molecular weights (kDa) are shown in brackets. See Supplementary Fig. S2 for additional details.

ADARs and RNA exosome components are in close proximity in the nucleus

Collectively, the affinity-tagged co-IPs (Fig. 2) and the endogenous co-IPs (Fig. 3) indicate interaction between ADARs and the RNA exosome that likely occur in the nucleus. To establish the subcellular localization of the ADAR–exosome interactions, we performed PLA [60]. For ADAR1 PLA experiments, antibodies recognizing endogenous ADAR1 or endogenous RNA exosome components EXOSC8, EXOSC9, EXOSC10, or hMTR4 and DHX9 were used (Fig. 4A, top). In this assay, proximal localization (<40 nm) of the targets allows for the generation of distinct fluorescent foci. Dual-antibody PLA yielded robust nuclear puncta for ADAR1 with each tested RNA-exosome protein (Fig. 4A, bottom and Supplementary Fig. S4). Negative controls with no primary antibody or matched IgG were at background level, whereas

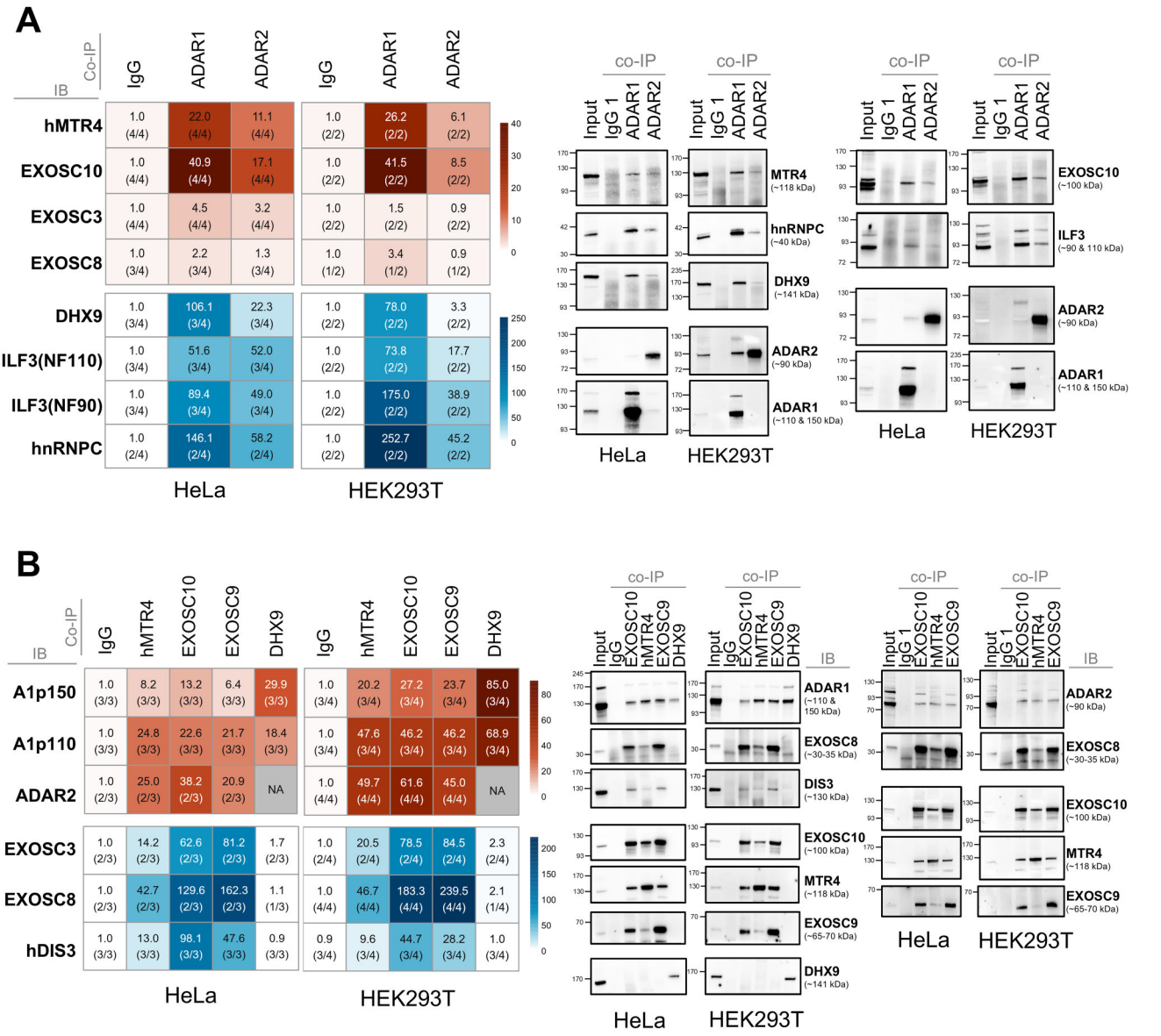

Figure 3. ADARs interact with RNA exosome components at the endogenous level. (**A**) Co-IP of endogenous ADARs. Lysates were co-IPed with anti-ADAR1 or anti-ADAR2 and probed for RNA-exosome subunits hMTR4, EXOSC10, EXOSC3, and EXOSC8 and known ADAR partners DHX9, ILF3, and hnRNPC. Left, quantitative heatmaps; right, representative immunoblots. (**B**) Reciprocal co-IP of RNA exosome components. Co-IPs with antibodies to hMTR4, EXOSC10, EXOSC9, and DHX9 were probed for ADAR1 and ADAR2. Heatmaps and blots are shown as in panel (A). Quantification and loading. Heatmaps report IgG-normalized intensities of the bound fraction (value in each tile); the fraction in parentheses indicates detection frequency across replicates; gray = not assayed. The color scale reflects enrichment, with red = novel interactors and blue = previously reported interactors. Immunoblots load inputs = 0.5% of lysate and bound = ½ of the eluate; a rabbit IgG isotype IP serves as a negative control for nonspecific binding. The predicted molecular weights (kDa) are shown in brackets. See Supplementary Fig. S3 for additional details.

the known ADAR1 interactor DHX9 produced abundant puncta, demonstrating assay specificity. Signals were predominantly nuclear as they were in DAPI-positive regions with minimal cytoplasmic staining, consistent with the subcellular distribution of ADARs and the exosome in the absence of IFN. Quantification confirmed a significant increase in foci per nucleus for the dual-antibody conditions versus controls (Fig. 4B). Among targets, EXOSC10 showed the highest mean foci per nucleus; DHX9, EXOSC9, and hMTR4 were strongly elevated, whereas EXOSC8 showed a moderate increase—a trend in agreement with the co-IP results.

In parallel, we investigated ADAR2 proximity to the RNA exosome complex. As multiple antibodies against endogenous ADAR2 lacked sufficient specificity in our hands, we generated doxycycline-inducible HeLa T-REx cells expressing SHN-ADAR2 WT protein (Fig. 4C, top). Upon induction, ADAR2 localized predominantly to the nucleus with nucleolar enrichment, as expected [11, 14] (Supplementary Fig. S4B). Proximity validation was performed with anti-HA to detect epitope-tagged ADAR2 together with antibodies against endogenous RNA-exosome components, EXOSC9 and EXOSC10, or the known ADAR2 interactor ILF3 (Fig. 4C, top). Upon doxycycline induction, SHN-ADAR2 produced robust PLA signals with EXOSC10, EXOSC9, and ILF3 (Fig. 4C, bottom and Supplementary Fig. S4C). The number and intensity of PLA foci varied between targets and even between

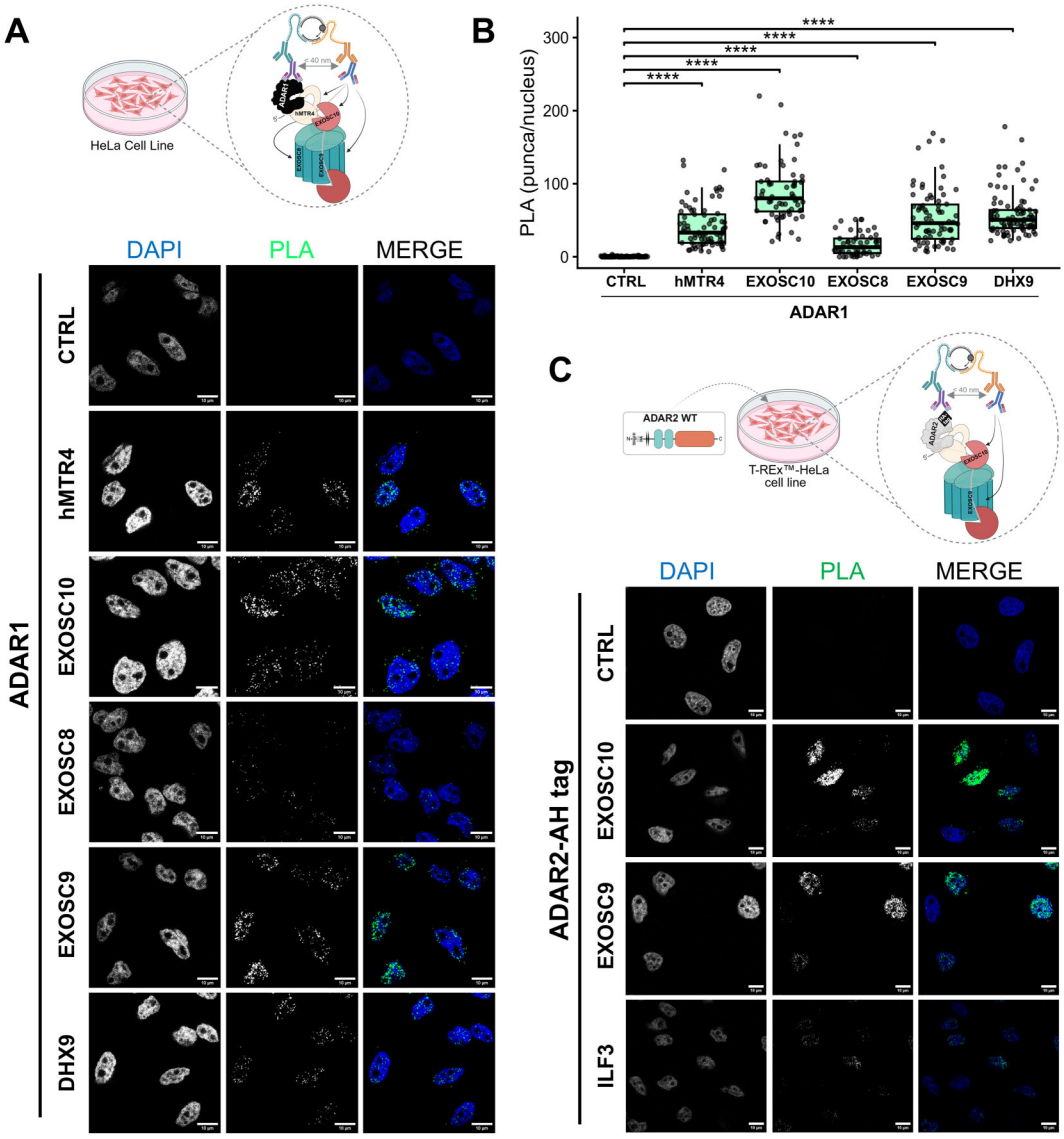

Figure 4. Nuclear proximity of ADAR proteins and RNA exosome components. (**A**) Top, schematic of the colocalization for ADAR1 and exosome with PLA. Created in BioRender. O'Connell, M. (2026) https://BioRender.com/qnquldo. HeLa cells were stained with ADAR1-specific and RNA-exosome-specific antibodies. Bottom, representative microcopy images of Duolink PLA in HeLa between endogenous ADAR1 protein and RNA exosome components, as shown in panel (A). Nuclei are stained with DAPI (blue) and positive interaction is represented with PLA foci (green). Individual channels are shown in grayscale for better visualization; scale bar, 10 μm. Negative controls included no primary antibody or the matched IgG. Additional microscopic images are provided in Supplementary Fig. S4A. (**B**) Quantification of panel (A): PLA puncta per nucleus (each dot = one nucleus). Counts were obtained in ImageJ (Particle Analysis). Statistics: Kruskal–Wallis followed by Mann–Whitney tests with Holm correction (****$P < .0001$). Biological replicates n = 3–4; >50 cells per condition. "CTRL" combines the two negative controls. (**C**) Top, schematic for the ADAR2 PLA. HeLa T-REx cells expressing StrepII–HA–ADAR2 were induced 24 h before PLA and stained with mouse anti-HA plus antibodies to exosome subunits. Created in BioRender. O'Connell, M. (2026) https://BioRender.com/qnquldo. As in panel (A), with tagged ADAR2 versus endogenous exosome components in HeLa T-REx cells. Representative images; scale and staining information as in panel (A). Further details are provided in Supplementary Fig. S4C.

nuclei on the same slide, from a few puncta to densely labeled nuclei, in all cases indicating strong level of interaction in the nucleus.

The variation in foci number detection likely reflects differences in ADAR2 expression under doxycycline induction or simply the inherent stochastic variability associated with efficient initial priming in PLA (Supplementary Fig. S4B).

In summary, ADAR1 and ADAR2 reside in close proximity to hMTR4 and multiple RNA exosome subunits in the nucleus, validating the co-IP results and supporting a robust association between ADARs and the RNA exosome in cells.

ADAR dsRNA-binding domains are required for interactions with RNA exosome components

To delineate regions of ADARs required for interaction with RNA exosome components, we expressed a series of SHN-tagged deletions of ADAR1 or ADAR2 and performed HA epitope-tagged co-IP, followed by immunoblotting for the RNA exosome components EXOSC3, EXOSC8, and EXOSC10, as well as hMTR4, and known interactors of ADARs such as DHX9, ILF2, and ILF3 (Fig. 5 and Supplementary Fig. S5). Heatmaps for ADAR1 (Fig. 5A, left) and ADAR2 (Fig. 5B, left) summarize mean signal intensities obtained

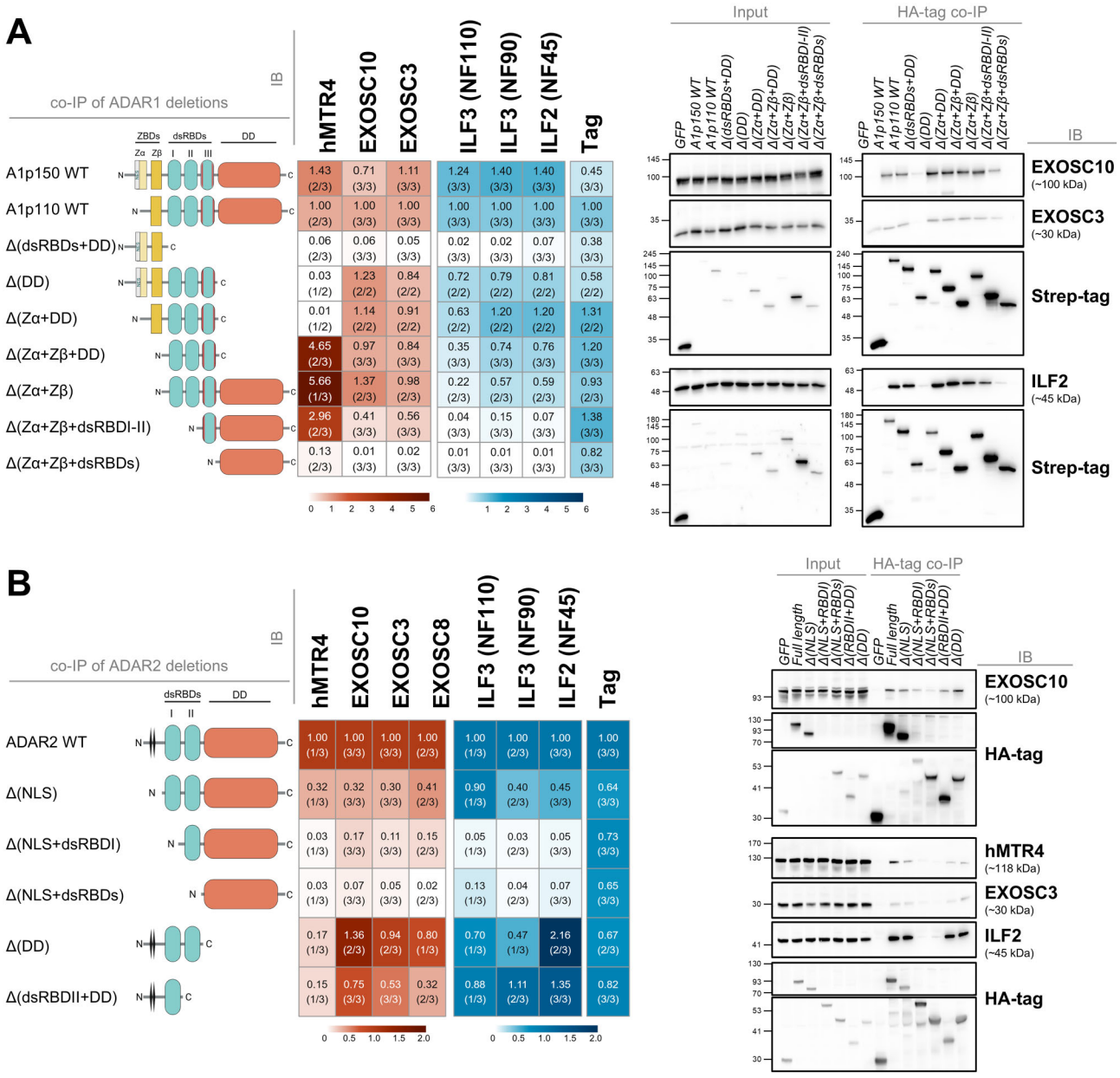

Figure 5. ADAR dsRBD domains are required for RNA exosome interaction. (**A**) Left, domain cartoons of the ADAR1 expressing plasmids used for co-IPs. Middle, heatmap summarizing co-IP signals for indicated preys (IB). Values are the mean signal normalized to the ADAR1p110-expressing plasmid and fractions in parentheses indicate contributing replicates (e.g. 2/3). Color gradient corresponds to the fold change (red-RNA exosome components and blue-known ADAR interactors). Right, representative cropped immunoblots of HA-tag co-IP from transiently transfected HEK293T showing inputs and anti-HA co-IPs probed with the indicated antibodies (IB); their predicted molecular weights (kDa) are shown in brackets an anti-HA blot confirms bait recovery. Created in BioRender. O'Connell, M. (2026) https://BioRender.com/qnquldo. (**B**) Left, domain cartoons of the ADAR2-expressing plasmids used for co-IP. Middle, heatmap as in panel (A), with values normalized to plasmid expressing full-length ADAR2. Replicate counts are shown in parentheses for each tile and color gradient as in panel (A). Right, representative cropped immunoblots of HA-tag co-IP from doxycycline-induced HEK293 T-REx stable cell lines showing inputs and anti-HA co-IPs probed with the indicated antibodies (IB); an anti-HA blot confirms bait recovery. Conserved domains for ADAR1 and ADAR2 are shown in different colors: ZDNA/RNA-binding domain (ZBD), dsRNA-binding domains I–III (dsRBDs), deaminase domain (DD), and nuclear localization signal (NLS) of ADAR1 are shown as two red lines overlapping dsRBD III, and NLS of ADAR2 is shown as two black lines at N-terminus; nuclear export signal (NES) found in ADAR1p150 is in gray. Created in BioRender. O'Connell, M. (2026) https://BioRender.com/qnquldo.

across all biological replicates normalized to the nuclear full-length bait, such as ADAR1p110 for the ADAR1-expressing plasmids or full-length ADAR2 for the ADAR2-expressing plasmids. Importantly, ADAR1's localization is determined by an NES at the N-terminus and a bimodular NLS overlapping the dsRBD III, which are depicted on the schematics as a gray rectangle and two red lines, respectively. Thus, ADAR1p150 WT, Δ(dsRBDs + DD), Δ(DD), and Δ(Zα+Zβ+dsRBDs) are expected to have predominantly a cytoplasmic localization, while the remainder of the plasmids expressing ADAR1p110 WT, Δ(Zα+DD), Δ(Zα+Zβ+DD), Δ(Zα+Zβ), and Δ(Zα+Zβ+dsRBDI-II) are expected to have a nuclear localization. On the other hand, ADAR2 localization is determined by an N-terminal NLS consisting of two highly conserved basic clusters, represented as black lines in the figure. So, the ADAR2-expressing plasmids Δ(NLS), Δ(NLS +

dsRBDI), and Δ(NLS + dsRBDs) are expected to have a cytoplasmic localization, while the ADAR2 WT, Δ(DD), and Δ(dsRBDII + DD) are expected to localize to the nucleus.

The minimum ADAR1 domain that interacts with the RNA exosome subunits and known interactors with minimal loss is the dsRBD III domain, in combination with other dsRBDs or the deaminase domain (Fig. 5A). This includes the following plasmids expressing Δ(DD), Δ(Zα+DD), Δ(Zα+Zβ+DD), Δ(Zα+Zβ), and Δ(Zα+Zβ+dsRBDI-II). By contrast, all tested interactors showed marked reductions in interaction with ADAR1 plasmids lacking the dsRBD III region and the NLS [Δ(dsRBDs + DD) and Δ(Zα+Zβ+dsRBDs)]. Interestingly, while there was an effect on interaction with the RNA exosome components when dsRBD I-II were absent [Δ(Zα+Zβ+dsRBDI-II)], this was stronger for known interactors ILF3 and ILF2. A similar pattern was observed for ADAR2 (Fig. 5B). Plasmids expressing dsRBD I with the N-terminal NLS retained strong recovery of EXOSC10, EXOSC8, EXOSC3, and MTR4. These include Δ(DD) and Δ(dsRBDII + DD)-expressing plasmids. Whereas the removal of the N-terminal segment harboring the NLS alone or in combination with the loss of dsRBDs [Δ(NLS), Δ(NLS + dsRBDI), and Δ(NLS + dsRBDs)] substantially diminished the RNA exosome signal. Loss of the ADAR1 or ADAR2 dsRNA-binding regions markedly reduced co-IP of ILF3 and ILF2, consistent with their RNA-bridged association with ADARs as reported in prior studies [20, 57]. This data indicates that the interaction between ADARs and components of the RNA exosome depends on dsRNA-binding and is influenced by nuclear localization of ADAR proteins.

Depletion of EXOSC3 suppresses the reduced reporter RNA levels in an MS2–MCP tethering assay that is ADAR-mediated

The MS2–MCP tethering system specifically recruits an MCP-tagged protein of interest to MS2 stem-loops that can, for example, be inserted into the 3′ UTR of a reporter construct to assess effects on mRNA metabolism [61, 62]. Such a system has been widely used to track mRNA life cycle events [63, 64], including for testing the effect of factors on mRNA stability and translation [65, 66]. To determine whether tethered ADARs modulate reporter's RNA stability or activity, we fused ADAR1p110, ADAR1p150, ADAR2, and their deletion variants in-frame with MCP that binds to MS2 hairpins in the 3′ UTR of a firefly luciferase reporter (Fig. 6A). Importantly, fusing MCP to the N-terminus of ADARs did not affect their editing activity as measured with an A-to-I-editing-dependent NanoLuc reporter [67] (Supplementary Fig. S6A), nor their subcellular localization (Supplementary Fig. S6B), nor protein stability and abundance (Supplementary Fig. S6C and D).

HEK293T cells were transiently co-transfected with ADAR–MCP constructs and the mirGLO reporter plasmid. After the incubation period (18–20 h), we quantified Firefly and Renilla reporter mRNA by RT–qPCR and measured enzyme activity with the Dual-Glo® luciferase assay. The introduction of ADAR1p110 or of ADAR2 caused a significant reduction in both luciferase reporter mRNA levels (Fig. 6B and C, qPCR) and luciferase activity (Fig. 6B and C, Dual-GLO luciferase assay) relative to GFP, consistent with tethering-induced mRNA decay. The minimal domain that retained strong repressive activity at levels comparable to their full-length counterparts were the dsRBDs with the Zβ for ADAR1 (Fig. 6B) and the dsRBDs with the NLS for ADAR2 (Fig. 6C). ADAR1–MCP constructs with the NLS reduced luciferase reporter mRNA, whereas those also containing the NES were less effective, indicating the nuclear effect on reporter repression (Fig. 6B). In most cases, luciferase activity mirrored changes in mRNA abundance, with two interesting exceptions. In ADAR1p150, the Δ(DD) construct, lacking the deaminase domain, but retaining Zα and NES, showed a significant decrease in activity without a corresponding reduction in mRNA levels (Fig. 6B). The same effect was not observed for ADAR1p110 and Δ(Zα+DD) constructs, both of which are located in the nucleus (Supplementary Fig. S6B).

In predominantly nuclear ADAR2, the cytoplasmic Δ(NLS) variant displayed a similar divergence, reducing luciferase activity more strongly than mRNA levels (Fig. 6C). Although mRNA and luciferase activity generally showed concordant trends, the overall reduction in protein output was often more pronounced, especially for constructs encoding variants predicted to be mostly cytoplasmic; ADAR1p150 versus A1p110, Δ(DD) versus Δ(Zα+DD), and A2 versus Δ(NLS), suggesting that tethered ADARs may also exert translational repression. Finally, full-length catalytically inactive and RNA-binding-defective mutants all reduced mRNA to a similar extent as WT, indicating that the effect on reporter is largely independent of deaminase activity and dsRNA binding via the dsRBDs (Supplementary Fig. S6E). Moreover, IFN induction, which upregulates the ADAR1p150 isoform, did not alter the outcome when compared with untreated cells (Supplementary Fig. S6E).

To test whether the ADAR-dependent reduction in reporter mRNA levels reflects RNA exosome-mediated decay, we depleted EXOSC3, which is a core exosome subunit, with siRNA (Fig. 6D). A scrambled siRNA (siCTRL) served as a negative control. As a further control, we also used siRNA targeting DIS3L2, a 3′→5′ exoribonuclease that operates independently of the RNA exosome [68]. Efficacy of depletion at 48 h post-transfection was confirmed by immunoblotting (Fig. 6D, left and Supplementary Fig. S6F). As observed previously, Firefly luciferase mRNA normalized to Renilla decreased upon ADAR1- or ADAR2-MCP tethering in siCTRL cells and remained decreased in DIS3L2-depleted cells (Fig. 6D, right). In contrast, EXOSC3 depletion significantly suppressed the downregulation of firefly luciferase mRNA level, indicating that the ADAR-tethering effect on the luciferase reporter mRNA is mediated by the RNA exosome.

In summary, the minimum domains of ADARs that match the effect of full-length proteins are dsRBD III together with the Zβ domain of ADAR1 and dsRBD I of ADAR2. These domains drive a decrease in firefly luciferase mRNA levels when artificially positioned on the 3′ UTR via the MS2–MCP system. This decrease is suppressed when EXOSC3, a core component of the RNA exosome complex, but not an unrelated enzyme DIS3L2, is depleted, indicating that the tethering of ADARs onto a reporter firefly construct via the MS2–MCP system results in its degradation by the RNA exosome.

ADAR is important for efficient 5.8S rRNA 3′-end maturation by the exosome and other aspects of ribosome biogenesis

Having established physical interaction between ADAR and the RNA exosome, and having provided initial ev-

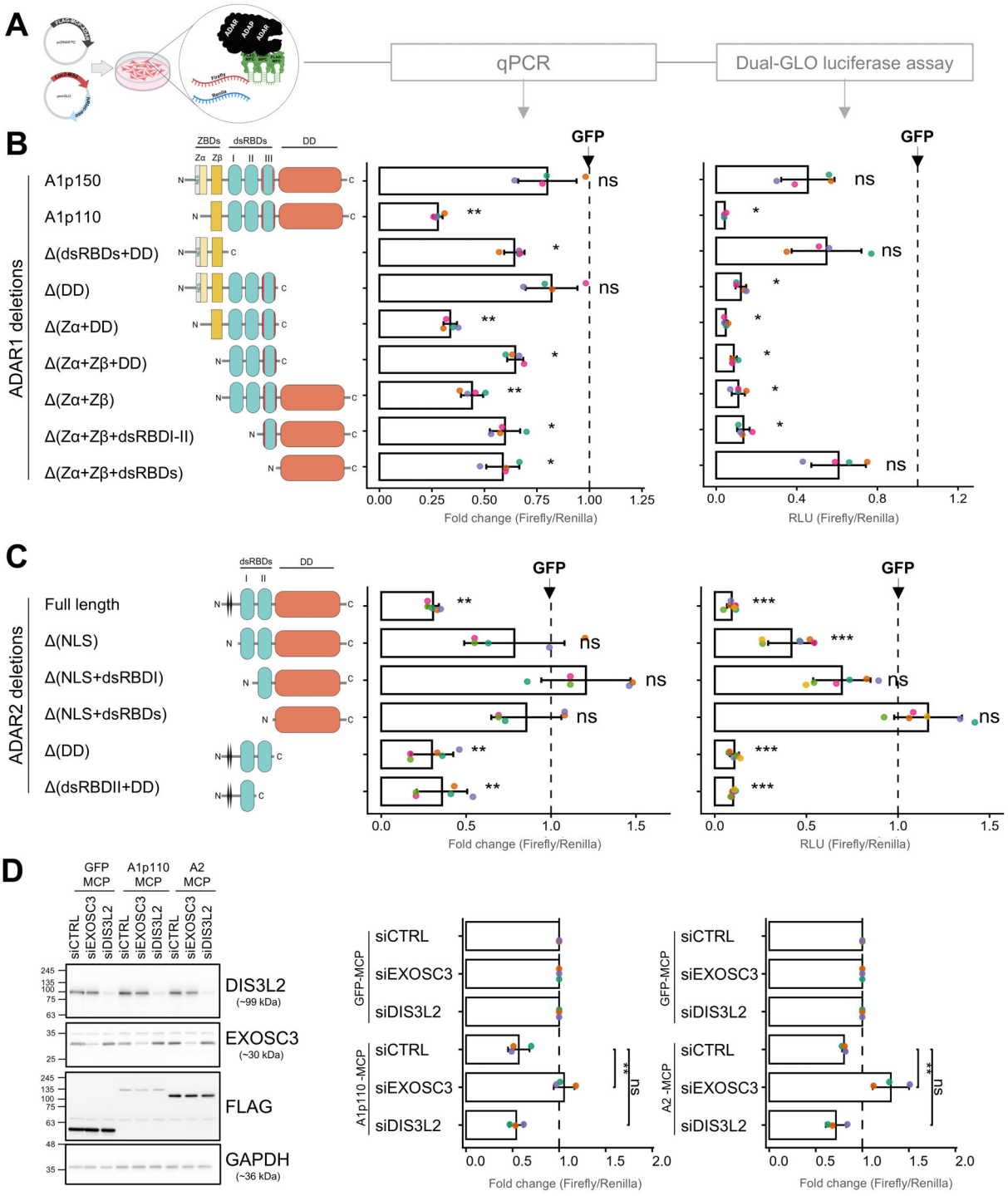

Figure 6. EXOSC3 knockdown prevents reporter mRNA decrease when ADARs are tethered via the MS2–MCP system. (**A**) Scheme depicting workflow. HEK293T cells were co-transfected with pmirGLO reporters encoding MS2 stem-loops in the 3′ UTR and ADAR–MCP fusion constructs (or GFP–MCP). After incubation, luciferase reporter mRNA levels were measured with RT–qPCR and luciferase activity with the Dual-Glo® luciferase assay. Firefly signals were normalized to Renilla and then to the appropriate GFP control condition. Created in BioRender. O'Connell, M. (2026) https://BioRender.com/qnquldo. (**B**) ADAR1–MCP tethering assay. Left, domain cartoons of ADAR1 expressing plasmids. Middle, RT–qPCR fold change relative to GFP–MCP (dashed line = 1). Right, Dual-Glo activity relative to GFP–MCP (dashed line = 1). For each plasmid, Firefly/Renilla was computed per replicate and normalized to the GFP–MCP mean of that experiment. Bars show mean ± SD with jittered points ($n = 4$–6 independent replicates). Statistics: Welch's ANOVA with Games–Howell post-hoc tests versus GFP–MCP; $P < .05$ (*), $P < .01$ (**), $P < .001$ (***), ns = not significant. Created in BioRender. O'Connell, M. (2026) https://BioRender.com/qnquldo. (**C**) ADAR2–MCP tethering. As in panel (B), but with ADAR2 deletion-expressing plasmids fused to MCP. Created in BioRender. O'Connell, M. (2026) https://BioRender.com/qnquldo. (**D**) HEK293T cells were transfected with CTRL, EXOSC3, or DIS3L2 siRNAs. After 30 h of siRNA transfection, cells were co-transfected with ADAR1/ADAR2–/GFP–MCP plus pmirGLO; analyses were performed at 48 h. Left, immunoblots showing target depletion and MCP-fusion expression; their predicted molecular weights (kDa) are shown in brackets. Right, Luciferase mRNA (qPCR) normalized to Renilla and expressed as fold change relative to CTRL (dashed line = 1). Bars represent mean ± SD from $n = 3$ biological replicates with individual points overlaid. Statistics: one-way ANOVA with Dunnett's tests versus CTRL; $P < .05$ (*), $P < .01$ (**), ns = not significant.

idence that these interactions are functionally significant using reporter construct, we next asked whether ADAR influences an endogenous, exosome-dependent processing step.

Specifically, we turned to the nucleolus, where ADAR localizes together with a very large fraction of its interactors (see Fig. 1C). We first examined its potential role in the formation of the 3′ end of 5.8S rRNA, a classical RNA exosome substrate on which this exoribonuclease complex was originally characterized [37]. The 3′-end maturation of 5.8S rRNA is a multistep process involving handover between subunits of the RNA exosome (depicted as a "Pacman" symbol in Fig. 7A) [69, 70]. Three reference cancer cell lines of distinct tissue origin—PaTu (pancreas), HeLa (cervix), and A549 (lung)—were treated for 2 days with silencers targeting ADAR1 or ADAR2 mRNAs. For ADAR1, we used both an esiRNA, consisting of a pool of silencers (ADAR1 #1), and a classical single-target siRNA (ADAR1 #2). For ADAR2, we used a single siRNA (ADAR2 #1). As controls, cells treated with a non-targeting scrambled siRNA, as well as untreated cells, were included (Fig. 7B). Total RNA was extracted and analyzed by northern blotting with a radioactively labeled probe, LD2079, that can detect all major precursors in the 3′-end processing pathway of 5.8S rRNA [71]. These include notably the 5.8S + 40 and 7S pre-rRNA, as well as other metastable intermediates (Fig. 7A). Upon ADAR depletion, we observed a clear accumulation of extended forms of 5.8S rRNA, which are natural substrates of the exosome, most notably the 7S precursor (Fig. 7B and C). This accumulation was particularly pronounced in PaTu and A549 cells treated with the ADAR1 esiRNA (ADAR1 #1). Prior to transfer, the denaturing acrylamide gel was stained with ethidium bromide, revealing the two known forms of 5.8S rRNA, where the short and long forms differ by a 7–8 nt 5′ extension, and the 5S rRNA. Despite inhibition of pre-rRNA processing, the steady-state levels of 5.8S rRNA were unchanged upon ADAR depletions. Importantly, the constant levels of 5S rRNA, which is an RNA polymerase III transcript, confirmed even loading between samples (Fig. 7B).

ADAR is enriched in the nucleolus, where it interacts with a diverse set of key ribosome assembly factors (see Fig. 1C). This prompted us to investigate more deeply its potential role in additional steps of ribosome biogenesis. Indeed, we obtained further evidence supporting a nucleolar function for ADAR, including subtle but highly reproducible effects on large ribosomal RNA processing (Supplementary Fig. S7A). Analysis of large pre-rRNA processing alterations upon ADAR knockdown in the early steps occurring in the 5′ external transcribed spacer (5′ ETS), which depend on the SSU-processome. The SSU-processome is a multi-megadalton nanomachine corresponding to the maturing small ribosomal subunit. It is best known as the "terminal balls" at the ends of the nascent RNA polymerase I transcripts on Miller chromatin spreads [72, 73]. Among the species examined, the 34S RNA was particularly informative. This RNA results from premature cleavage within internal transcribed spacer 1 (ITS1), which separates the 18S and 5.8S sequences of the 47S primary transcript (see Supplementary Fig. S7A). Under normal conditions, processing proceeds sequentially from the 5′ end of the polycistronic transcript, beginning in the 5′ ETS at sites 01, A0, and 1. If cleavage occurs first in ITS1, cells produce the aberrant 34S species (depicted in red in Supplementary Fig. S7A). Interestingly, steady-state levels of 34S vary among cell types: it is essentially undetectable in PaTu and HeLa cells (mock, SCR), but readily observed in A549 cells. Under ADAR perturbation, the observations can be summarized as follows: (i) in PaTu cells, detection of 34S upon ADAR2 depletion, which is accompanied by increased 30S; (ii) in A549 cells, reduction of 34S is observed upon ADAR1 depletion (with both silencers used); (iii) in HeLa cells, 34S levels are unchanged, but 30S is increased upon ADAR2 depletion, similar to what is observed with PaTu cells. Although these differences are subtle and cell-type-specific, they are highly reproducible and were observed in three biological replicates in experiments performed several months apart (Supplementary Fig. S7A). Altogether, these results indicate that early pre-rRNA processing is affected by ADAR.

Lastly, we examined whether ADAR influences the levels of specific 2′-O-methylations in rRNA. The rationale was that, if ADARs impact ribosome biogenesis kinetics, as suggested by the pre-rRNA processing alterations described earlier, this could in turn affect the efficiency of 2′-O-methylation at specific positions, for example by altering the time window during which a given substrate site is accessible. Each human ribosome contains between 106 and 112 nucleotides that are specifically 2′-O-methylated during nucleolar ribosomal subunit assembly by small nucleolar RNA-based machineries [74]. These modifications can be quantitatively assessed by deep sequencing with RiboMeth-seq (RMS) [74, 75]. Applying this assay to the RNA samples described above, we found that most positions were unaffected by ADAR depletion (Supplementary Fig. S7B and Supplementary Table S1). MethScore values were highly consistent between mock-treated and scrambled (SCR) control samples (ΔMethScore range: −0.04 to +0.05 across all rRNA positions), confirming the low technical noise and robustness of the assay (Supplementary Table S1). In contrast, ADAR-depleted samples displayed broader MethScore fluctuations relative to SCR controls (ΔMethScore range: −0.25 to +0.23), indicating that knockdown of ADAR enzymes induces discrete yet measurable local perturbations in rRNA modification. Despite these local effects, the global MethScore distribution remained highly similar across all samples, irrespective of ADAR depletion. Violin plot statistics further confirmed that the overall methylation landscape was preserved (Supplementary Fig. S7B). Notwithstanding this global stability, a subset of individual sites exceeded a variation threshold of $|\Delta\text{MethScore}| > 0.10$ (Fig. 7D and Supplementary Fig. S7C). These sites were distributed across both 18S and 28S rRNAs and included positions where depletion of either ADAR1 or ADAR2 resulted in decreased methylation (e.g. 18S_468, 28S_2861) or increased methylation levels (e.g. 18S_1440, 28S_2415), depending on the ADAR isoform targeted. Notably, several sites displayed ADAR1-specific effects (e.g. 18S_354, 18S_468, and 18S_627), whereas ADAR2 depletion affected a partially distinct subset (e.g. 28S_400).

In conclusion, ADAR, which is prominently localized in the nucleolus and, as shown here, interacts with a wide range of nucleolar proteins, including key ribosome assembly factors, plays an important role in (i) efficient 5.8S rRNA processing, consistent with its interaction with the RNA exosome; (ii) 5′ ETS maturation, consistent with its interaction with XRN2; and (iii) influencing rRNA methylation at specific sites, likely reflecting changes in the kinetics of ribosomal subunit assembly.

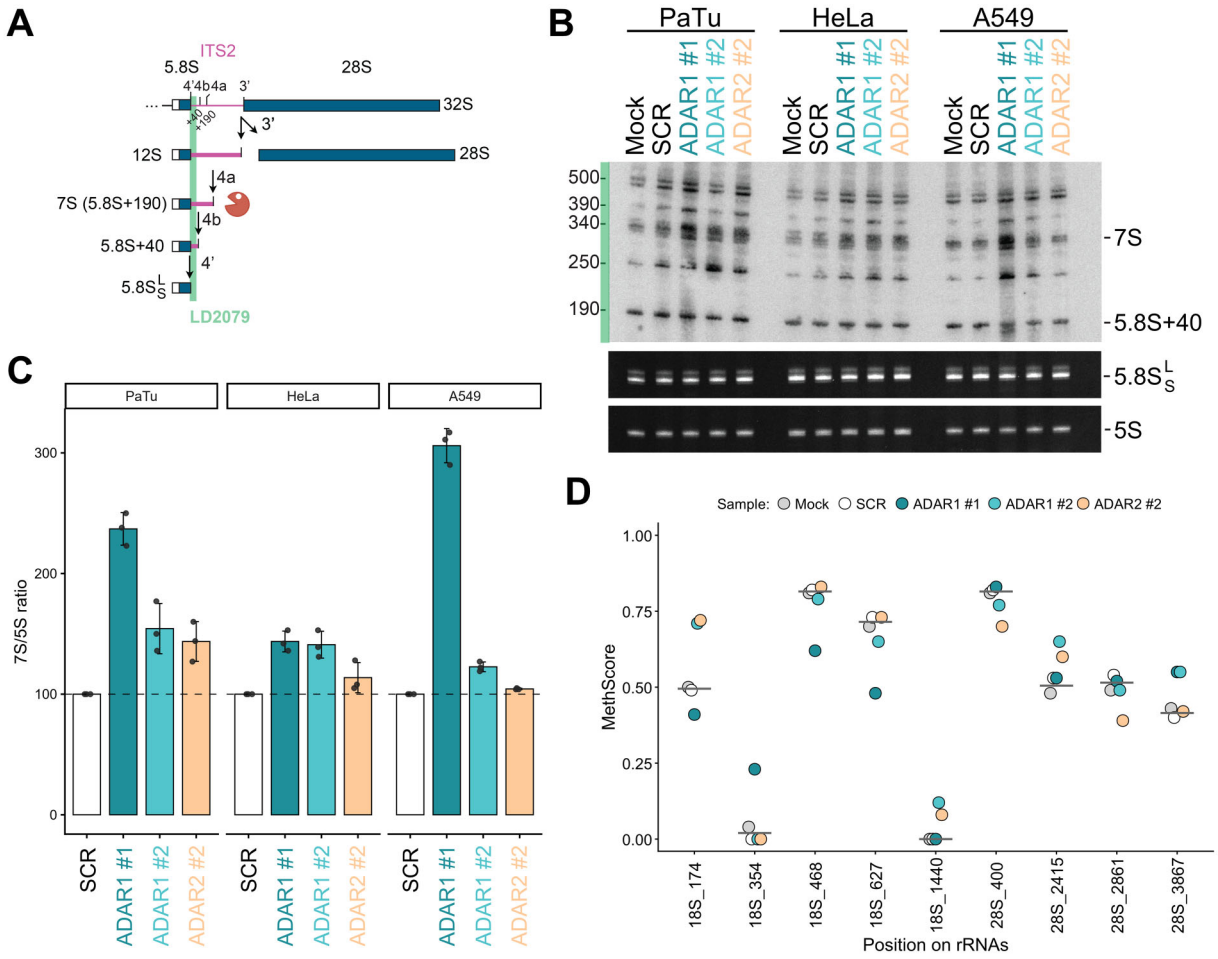

Figure 7. ADARs contribute to efficient 3′-end maturation of 5.8S rRNA. (**A**) Processing in ITS2. Major processing steps are indicated. The RNA exosome is depicted as a Pac-Man symbol. The probe used in panel (A) (LD2079) is shown. (**B**) northern blot analysis (denaturing acrylamide gels). Ethidium-stained gels revealed the two forms of 5.8S rRNA (short and long, differing by a 7–8 nt 5′ extension) as well as the 5S rRNA, confirming equal loading across samples. Silencing was performed for 2 days with 30 nM siRNAs targeting ADAR1, ADAR2, or scrambled siRNA. (**C**) Quantification of 7S pre-rRNA. Levels of the 7S precursor (a Pol I transcript) were quantified and normalized to 5S rRNA (a Pol III transcript). (**D**) Selected rRNA sites showing notable MethScore changes across mock, scrambled siRNA (SCR), ADAR1-depleted (esiRNA and siRNA), and ADAR2-depleted cells; values correspond to the MethScore at the indicated 18S or 28S rRNA positions.

Discussion

In this study, we identified an interaction between ADAR proteins and the nuclear RNA exosome, the major 3′–5′ RNA degradation machinery in the nucleus. Our results reveal that in addition to RNA editing ADAR proteins can also promote exosome-dependent RNA decay, linking RNA editing to nuclear RNA surveillance pathways.

Analysis of the stable ADAR2 interactome revealed multiple exosome subunits. The RNA exosome typically functions as a complex composed of a catalytically inert nine-subunit core and associated nuclease as core components, and different layers of cofactors and adaptors [27]. Although all nine core components were detected in the ADAR2 interactome dataset, only four subunits—EXOSC2, EXOSC3, EXOSC5, and EXOSC8—together with the ribonuclease EXOSC10 met stringent high-confidence criteria after filtering. Similar partial recovery of the RNA exosome complex has been reported for other exosome-associated adaptors [25, 76]. Our filtering criteria also excluded the known ADAR2 interactor STRBP [20], suggesting that a few bona fide interactions fall below high-confidence threshold. While EXOSC10 has repeatedly appeared in ADARs interaction datasets [20–23], the catalytic subunit DIS3 was not detected in our co-IP/MS analysis but has been reported as an HCI in ADAR1 BioID experiment [21]. This discrepancy likely reflects the dynamic association of DIS3 with the exosome core, which can dissociate during purification [77–79]. Comparison between our newly established ADAR2 interactome and published ADAR1 interactomes revealed overlapping RNA exosome components, suggesting that association with the RNA exosome is a conserved feature of both ADAR proteins. Our findings are corroborated by several previous high-throughput studies that employed either ADARs or RNA exosome components as bait and reported similar links but did not explore these interactions further [20–25]. Thus, our results provide the first mechanistic evidence that ADAR proteins interact with the RNA exosome, expanding their biological function beyond A-to-I editing.

Interactions were confirmed by co-IP experiments with epitope-tagged ADAR1p110, ADAR1p150, and ADAR2 and several RNA exosome components: EXOSC10, EXOSC3, and EXOSC8, as well as helicase hMTR4, with the strength of the interaction varying between ADAR proteins and individual exosome subunits. Co-IP of endogenous ADAR1 and ADAR2 proteins recovered RNA exosome subunits, and

reciprocal co-IPs with exosome subunits as bait confirming the presence of both ADAR1 and ADAR2, supporting that these associations occur under physiological conditions. ADAR1p110 and ADAR2 showed comparable enrichments, whereas ADAR1p150 was detected more weakly, consistent with its lower basal abundance. The ADAR–RNA exosome interaction was resistant to RNase A treatment. Although RNase resistance can suggest direct protein–protein contacts, mutations disrupting dsRNA binding in ADAR dsRBDs [59] abolished association with exosome components, indicating that RNA binding is required. Consistently, deletion mapping showed that the minimal regions sufficient for interaction include the dsRBDs together with their nuclear localization signals. A similar behavior has been reported for the dsRBD-containing protein, DGCR8, which interacts with EXOSC10 in a dsRBD-dependent but RNase-resistant manner [76]. Together, these observations suggest that ADAR–exosome association likely occurs on structured RNA substrates. As dsRBD mutants also alter ADAR subcellular localization [21], we cannot exclude that spatial redistribution contributes to the loss of interaction.

MS2–MCP tethering assays demonstrated that prolonged binding of ADAR proteins can promote RNA exosome-dependent decay. Tethering either ADAR1 or ADAR2 to a luciferase reporter transcript reduced both mRNA abundance and reporter activity. This effect was reversed upon EXOSC3 depletion, indicating that the destabilization requires RNA exosome activity. Catalytically inactive ADAR mutants produce similar effects, supporting an editing-independent mechanism. These results extend previous observations that ADAR proteins regulate RNA abundance via multiple mechanisms [34–36]. PLA further supported nuclear proximity between ADAR proteins and RNA exosome components. The PLA signals were distributed throughout the nucleus and displayed heterogeneous spatial distribution, including regions adjacent to the nucleolus as well as nucleoplasmic foci. The requirement of dsRBDs in co-IP experiments raises the possibility that ADARs and exosome components co-localize within defined, RNA-rich nuclear compartments [80–83]. ADAR proteins are known to dynamically partition into several cellular compartments rich in RNA, including nucleoli [6, 11, 21], stress granules [84, 85], RNase L-dependent bodies [86], and dsRNA-induced foci [87]. RNA is recognized as a key organizer of such biomolecular condensates, where structured RNAs can nucleate assemblies of RNA-binding proteins [88]. However, our PLA experiments cannot determine whether the observed foci represent phase-separated condensates. Recent work supports the idea that RNA-driven assemblies can organize RNA surveillance pathways in context of dsRNA/R-loops during stress [89]. In particular, in addition to belonging to the baseline MYC interactome, ADAR1 and RNA exosome components were detected in stress-induced MYC multimers. These assemblies suppress accumulation of immunogenic RNA species and limit innate immune activation. Thus, the physical association between ADAR proteins and RNA exosome components described here provides a potential mechanistic link between RNA editing and RNA degradation within such RNA surveillance hubs.

One prominent compartment relevant to this interaction is the nucleolus, a major RNA-rich nuclear condensate responsible for rRNA transcription and ribosome assembly [82]. Both ADAR1 and ADAR2 accumulate in nucleolus and dynamically exchange with the nucleoplasm [11, 14, 90]. Nucleolar localization has been proposed to regulate ADAR activity as perturbations such as substrate expression [11] or nucleolar disassembly [15] redistribute ADARs and correlate with altered editing outcomes and pre-mRNA splicing rewiring. Consistent with this context, ADAR depletion perturbs nucleolar homeostasis and affects several aspects of ribosome biogenesis, including pre-rRNA processing and modification. In particular, we observed effects on the 3′-end maturation of 5.8S rRNA, a well-established RNA exosome substrate and the substrate on which the RNA exosome was originally identified [37], as well as accumulation of 34S pre-rRNA linked to ADAR interaction with the 5′–3′ exonuclease XRN2 [52, 71, 91]. These provide functional insight into the physical interactions between ADAR and nucleolar proteins reported here and elsewhere [21] and RNAs [92]. Thus, the physical and functional interactions we describe here between ADARs and exosome components provide a plausible mechanistic basis for these effects: ADARs may recognize structured rRNA precursor elements and facilitate their engagement with exosome-associated ribosome biogenesis factors. We emphasize that pre-rRNA processing was examined as a physiological test of ADAR–exosome function on endogenous exosome substrates. The observed effects were modest, and we therefore interpret them cautiously as evidence of a contributory rather than essential role of ADARs in nucleolar RNA metabolism. Likewise, site-specific changes in rRNA 2′-O-methylation likely reflect indirect consequences of altered processing kinetics rather than a direct role in rRNA modification.

Beyond rRNA, our findings raise the broader question of which other endogenous RNAs rely on the ADAR–exosome interaction. The requirement for intact dsRNA-binding domains suggests that structured RNA plays a central role in this process. This parallels the role of DGCR8, which binds structured RNAs and cooperates with EXOSC10 to regulate the levels of mature snoRNAs and human telomerase RNA (hTR) [76] or interaction of microprocessor complex with the vNEXT complex targeting some stem-loop-containing RNAs [93]. Consistent with the known preference of ADAR proteins for long dsRNAs, such as those formed by inverted Alu repeats [18, 94], while the exosome degrades structured, aberrant, or improperly processed RNAs (for review [27]). Coupling these activities could provide a mechanism for nuclear quality control of endogenous dsRNA. Such cooperation may help limit the accumulation of immunogenic endogenous dsRNA, as both ADAR editing and RNA exosome-mediated decay prevent inappropriate activation of immune response [4, 89, 95, 96]. In this model, ADAR proteins, in addition to editing, act as sensors of specific structured RNA and facilitate recruitment of the exosome to limit their accumulation and the activation of the innate immune response (for review [4]). The presence of the helicase MTR4 among ADAR interactors supports this, as MTR4 likely promotes unwinding and degradation of structured RNA substrates prior to exosome degradation [77]. Furthermore, both ADARs and the RNA exosome have been implicated in the metabolism of RNA:DNA hybrids, R-loops, and genome stability pathways [97]. MTR4 and EXOSC10 can process RNA:DNA hybrids [98–102], and ADARs have been shown to regulate R-loop/DNA:RNA hybrid formation and replication stress responses [103–105]. These observations raise the possibility that ADAR–exosome cooperation contributes to the turnover of RNA structures associated with transcription or DNA damage.

The interaction between ADARs and the RNA exosome may also help explain several observations in site-specific RNA editing. Many site-specific editing sites occur near the 3′ end of exons close to 5′ splice sites, where duplexes formed with downstream introns must be removed by splicing before they attract RNA decay pathways. Consistently, constructs designed to mimic endogenous editing sites perform best when they do not form very stable duplexes. Accordingly, circular ADAR-recruiting RNAs, which are more resistant to RNA decay, are now commonly used to achieve efficient site-specific editing [106].

In summary, we identify ADAR1 and ADAR2 as previously unrecognized partners of the nuclear RNA exosome and show that this association influences RNA stability and processing. Our data support a model in which ADAR proteins recognize structured RNA substrates through their dsRBDs and facilitate their engagement with the RNA exosome degradation machinery. These findings expand the functional landscape of ADAR proteins beyond RNA editing and suggest that ADARs may contribute more broadly to nuclear RNA surveillance pathways that control structured and potentially immunogenic RNAs. Key questions for future work include how substrates are selected for ADAR-assisted decay, whether RNA editing modulates exosome recruitment or substrate choice, and how disruption of this pathway contributes to human disease.

Acknowledgements

We acknowledge the core facility CELLIM, supported by the Czech-BioImaging large RI project (LM2023050 funded by MEYS CR), for their support with obtaining scientific data presented in this paper. We thank the Viikki Proteomics Unit (of the Helsinki Proteomics Center) supported by the University of Helsinki, Biocenter Finland, and HiLIFE. We thank Štěpánka Vaňáčová, Nandan Mysore Varadarajan, and Helena Covelo Molares for their valuable insightful discussions. We also thank Katarína Repiská for assistance with some experimental work. The graphical abstract was created in BioRender. O'Connell, M. (2026) https://BioRender.com/qnquldo.

Author contributions: Dragana Vukić (Conceptualization [lead], Data curation [equal], Formal analysis [equal], Investigation [equal], Methodology [equal], Writing – original draft [equal], Writing – review & editing [equal]), QiuPei Du (Data curation [equal], Formal analysis [equal], Investigation [equal], Methodology [equal], Writing – original draft [equal], Writing – review & editing [equal]), Anna Cherian (Investigation [equal], Methodology [equal], Writing – review & editing [equal]), Damiano Amoruso (Investigation [supporting], Methodology [supporting], Writing – review & editing [supporting]), Květoslava Brožinová (Investigation [supporting], Methodology [supporting], Writing – review & editing [supporting]), Ludivine Wacheul (Investigation [equal], Methodology [equal], Writing – review & editing [equal]), Valentina Lacovich (Investigation [equal], Methodology [equal], Writing – review & editing [equal]), Christiane Zorbas (Investigation [equal], Methodology [equal]), Leena Yadav (Investigation [equal], Methodology [equal], Writing – review & editing [equal]), Jiří Sedmík (Investigation [equal], Methodology [equal], Writing – review & editing [equal]), Salla Keskitalo (Investigation [equal], Methodology [equal], Writing – review & editing [equal]), Khadija Hajji (Investigation [equal], Methodology [equal], Writing – review & editing [equal]), Stanislav Stejskal (Investigation [equal], Methodology [equal], Writing – review & editing [equal]), Markku Varjosalo (Formal analysis [equal], Funding acquisition [equal], Project administration [equal], Writing – review & editing [equal]), Denis L.J. Lafontaine (Formal analysis [equal], Funding acquisition [equal], Investigation [equal], Writing – review & editing [equal]), Liam P. Keegan (Formal analysis [equal], Funding acquisition [equal], Writing – review & editing [equal]), and Mary A. O'Connell (Conceptualization [lead], Formal analysis [lead], Funding acquisition [lead], Project administration [lead], Writing – original draft [supporting], Writing – review & editing [supporting])

Supplementary data

Supplementary data is available at NAR online.

Conflict of interest

None declared.

Funding

This work was also supported by a grant from the Czech Science Foundation GAČR 21-27329X to M.A.O'C. D.V. was supported by GAČR 20-11101S and GAČR 24-12635S. Research in the laboratory of D.L.J.L. was supported by the Belgian Fonds de la Recherche Scientifique (F.R.S.-FNRS), EOS (CD-INFLADIS, 40007512), Région Wallonne (SPW EER) Win4SpinOff (RIBOGENESIS), the COST Action TRANSLACORE (CA21154), the European Joint Programme on Rare Diseases (EJP-RD): RiboEurope and DBAGeneCure, and the Marie Skłodowska-Curie Actions Doctoral Network (MSCA-DN) EURECA (https://eureca-dn.com/). Research in the laboratory of M.V. was funded by the Academy of Finland (nos. 288475 and 294173) to M.V., the Sigrid Jusélius Foundation, the Finnish Cancer Foundation, Biocenter Finland, and HiLIFE. Funding to pay the Open Access publication charges for this article was provided by Masaryk University.

Data availability

The mass spectrometry proteomics data have been deposited to the ProteomeXchange Consortium via the PRIDE [107] partner repository with the dataset identifier PXD071677. Sequencing data were deposited in GEO under accession number GSE322613.

References

1. Cappannini A, Ray A, Purta E *et al.* MODOMICS: a database of RNA modifications and related information. 2023 update. *Nucleic Acids Res* 2024;52:D239–44. https://doi.org/10.1093/nar/gkad1083
2. Goldeck M, Gopal A, Jantsch MF *et al.* How RNA editing keeps an I on physiology. *Am J Physiol Cell Physiol* 2022;323:C1496–511. https://doi.org/10.1152/ajpcell.00191.2022
3. Schaffer AA, Levanon EY. ALU A-to-I RNA editing: millions of sites and many open questions. *Methods Mol Biol* 2021;2181:149–62.

4. Quin J, Sedmík J, Vukić D *et al.* ADAR RNA modifications, the epitranscriptome and innate immunity. *Trends Biochem Sci* 2021;46:758–71. https://doi.org/10.1016/j.tibs.2021.02.002
5. Patterson JB, Samuel CE. Expression and regulation by interferon of a double-stranded-RNA-specific adenosine deaminase from human cells: evidence for two forms of the deaminase. *Mol Cell Biol* 1995;15:5376–88. https://doi.org/10.1128/MCB.15.10.5376
6. Strehblow A, Hallegger M, Jantsch MF. Nucleocytoplasmic distribution of human RNA-editing enzyme ADAR1 is modulated by double-stranded RNA-binding domains, a leucine-rich export signal, and a putative dimerization domain. *MBoC* 2002;13:3822–35. https://doi.org/10.1091/mbc.e02-03-0161
7. Barraud P, Banerjee S, Mohamed WI *et al.* A bimodular nuclear localization signal assembled via an extended double-stranded RNA-binding domain acts as an RNA-sensing signal for transportin 1. *Proc Natl Acad Sci USA* 2014;111:E1852–61. https://doi.org/10.1073/pnas.1323698111
8. Banerjee S, Barraud P. Functions of double-stranded RNA-binding domains in nucleocytoplasmic transport. *RNA Biol* 2014;11:1226–32. https://doi.org/10.4161/15476286.2014.972856
9. Poulsen H, Nilsson J, Damgaard CK *et al.* CRM1 mediates the export of ADAR1 through a nuclear export signal within the Z-DNA binding domain. *Mol Cell Biol* 2001;21:7862–71. https://doi.org/10.1128/MCB.21.22.7862-7871.2001
10. Hajji K, Sedmik J, Cherian A *et al.* ADAR2 enzymes: efficient site-specific RNA editors with gene therapy aspirations. *RNA* 2022;28:1281–97. https://doi.org/10.1261/rna.079266.122
11. Desterro JMP, Keegan LP, Lafarga M *et al.* Dynamic association of RNA-editing enzymes with the nucleolus. *J Cell Sci* 2003;116:1805–18. https://doi.org/10.1242/jcs.00371
12. Behm M, Wahlstedt H, Widmark A *et al.* Accumulation of nuclear ADAR2 regulates adenosine-to-inosine RNA editing during neuronal development. *J Cell Sci* 2017;130:745–53. https://doi.org/10.1242/jcs.200055
13. Wong SK, Sato S, Lazinski DW. Elevated activity of the large form of ADAR1 in vivo: very efficient RNA editing occurs in the cytoplasm. *RNA* 2003;9:586–98. https://doi.org/10.1261/rna.5160403
14. Sansam CL, Wells KS, Emeson RB. Modulation of RNA editing by functional nucleolar sequestration of ADAR2. *Proc Natl Acad Sci USA* 2003;100:14018–23. https://doi.org/10.1073/pnas.2336131100
15. Lattuca R, Bascetin R, Detours V *et al.* Systematic analysis of A-to-I RNA editing upon release of ADAR from the nucleolus. *RNA Biol* 2025;22:1–18. https://doi.org/10.1080/15476286.2025.2515655
16. Licht K, Hartl M, Amman F *et al.* Inosine induces context-dependent recoding and translational stalling. *Nucleic Acids Res* 2019;47:3–14. https://doi.org/10.1093/nar/gky1163
17. Higuchi M, Single FN, Kohler M *et al.* RNA editing of AMPA receptor subunit GluR-B: a base-paired intron-exon structure determines position and efficiency. *Cell* 1993;75:1361–70. https://doi.org/10.1016/0092-8674(93)90622-W
18. Bazak L, Haviv A, Barak M *et al.* A-to-I RNA editing occurs at over a hundred million genomic sites, located in a majority of human genes. *Genome Res.* 2014;24:365–76. https://doi.org/10.1101/gr.164749.113
19. Maronek M, Lacovich V, Cherian A *et al.* ADAR1: beyond Just an RNA Editor. *Annu Rev Cell Dev Biol* 2025;41:529–51. https://doi.org/10.1146/annurev-cellbio-101323-020352
20. Freund EC, Sapiro AL, Li Q *et al.* Unbiased identification of trans regulators of ADAR and A-to-I RNA editing. *Cell Rep* 2020;31:107656. https://doi.org/10.1016/j.celrep.2020.107656
21. Vukic D, Cherian A, Keskitalo S *et al.* Distinct interactomes of ADAR1 nuclear and cytoplasmic protein isoforms and their responses to interferon induction. *Nucleic Acids Res* 2024;52:14184–204. https://doi.org/10.1093/nar/gkae1106
22. Cottrell KA, Ryu S, Pierce JR *et al.* Induction of viral mimicry upon loss of DHX9 and ADAR1 in breast cancer cells. *Cancer Res Commun* 2024;4:986–1003. https://doi.org/10.1158/2767-9764.CRC-23-0488
23. Hong H, An O, Chan THM *et al.* Bidirectional regulation of adenosine-to-inosine (A-to-I) RNA editing by DEAH box helicase 9 (DHX9) in cancer. *Nucleic Acids Res* 2018;46:7953–69. https://doi.org/10.1093/nar/gky396
24. Hein MY, Hubner NC, Poser I *et al.* A human interactome in three quantitative dimensions organized by stoichiometries and abundances. *Cell* 2015;163:712–23. https://doi.org/10.1016/j.cell.2015.09.053
25. Lubas M, Christensen MS, Kristiansen MS *et al.* Interaction profiling identifies the human nuclear exosome targeting complex. *Mol Cell* 2011;43:624–37. https://doi.org/10.1016/j.molcel.2011.06.028
26. Kilchert C, Wittmann S, Vasiljeva L. The regulation and functions of the nuclear RNA exosome complex. *Nat Rev Mol Cell Biol* 2016;17:227–39. https://doi.org/10.1038/nrm.2015.15
27. Keidel A, Long CL, Iwasa J *et al.* RNA-degrading exosome complexes: molecular mechanisms and structural insights. *Annu Rev Cell Dev Biol* 2025;41:505–28. https://doi.org/10.1146/annurev-cellbio-111822-115115
28. Weick EM, Lima CD. RNA helicases are hubs that orchestrate exosome-dependent 3′–5′ decay. *Curr Opin Struct Biol* 2021;67:86–94. https://doi.org/10.1016/j.sbi.2020.09.010
29. Lubas M, Andersen PR, Schein A *et al.* The human nuclear exosome targeting complex is loaded onto newly synthesized RNA to direct early ribonucleolysis. *Cell Rep* 2015;10:178–92. https://doi.org/10.1016/j.celrep.2014.12.026
30. Hrossova D, Sikorsky T, Potesil D *et al.* RBM7 subunit of the NEXT complex binds U-rich sequences and targets 3′-end extended forms of snRNAs. *Nucleic Acids Res* 2015;43:4236–48. https://doi.org/10.1093/nar/gkv240
31. Meola N, Domanski M, Karadoulama E *et al.* Identification of a nuclear exosome decay pathway for processed transcripts. *Mol Cell* 2016;64:520–33. https://doi.org/10.1016/j.molcel.2016.09.025
32. Ogami K, Richard P, Chen Y *et al.* An Mtr4/ZFC3H1 complex facilitates turnover of unstable nuclear RNAs to prevent their cytoplasmic transport and global translational repression. *Genes Dev.* 2017;31:1257–71. https://doi.org/10.1101/gad.302604.117
33. Silla T, Karadoulama E, Makosa D *et al.* The RNA exosome adaptor ZFC3H1 functionally competes with nuclear export activity to retain target transcripts. *Cell Rep* 2018;23:2199–210. https://doi.org/10.1016/j.celrep.2018.04.061
34. Anantharaman A, Tripathi V, Khan A *et al.* ADAR2 regulates RNA stability by modifying access of decay-promoting RNA-binding proteins. *Nucleic Acids Res* 2017;45:4189–201. https://doi.org/10.1093/nar/gkw1304
35. Wang IX, So E, Devlin JL *et al.* ADAR regulates RNA editing, transcript stability, and gene expression. *Cell Rep* 2013;5:849–60. https://doi.org/10.1016/j.celrep.2013.10.002
36. Sakurai M, Shiromoto Y, Ota H *et al.* ADAR1 controls apoptosis of stressed cells by inhibiting Staufen1-mediated mRNA decay. *Nat Struct Mol Biol* 2017;24:534–43. https://doi.org/10.1038/nsmb.3403
37. Mitchell P, Petfalski E, Tollervey D. The 3′ end of yeast 5.8S rRNA is generated by an exonuclease processing mechanism. *Genes Dev.* 1996;10:502–13. https://doi.org/10.1101/gad.10.4.502
38. Varjosalo M, Sacco R, Stukalov A *et al.* Interlaboratory reproducibility of large-scale human protein-complex analysis by standardized AP-MS. *Nat Methods* 2013;10:307–14. https://doi.org/10.1038/nmeth.2400
39. Yadav L, Tamene F, Goos H *et al.* Systematic analysis of human protein phosphatase interactions and dynamics. *Cell Syst* 2017;4:430–44.

40. Kong AT, Leprevost FV, Avtonomov DM *et al.* MSFragger: ultrafast and comprehensive peptide identification in mass spectrometry-based proteomics. *Nat Methods* 2017;14:513–20. https://doi.org/10.1038/nmeth.4256
41. Yu F, Haynes SE, Teo GC *et al.* Fast quantitative analysis of timsTOF PASEF data with MSFragger and IonQuant. *Mol Cell Proteomics* 2020;19:1575–85. https://doi.org/10.1074/mcp.TIR120.002048
42. da Veiga Leprevost F, Haynes SE, Avtonomov DM *et al.* Philosopher: a versatile toolkit for shotgun proteomics data analysis. *Nat Methods* 2020;17:869–70. https://doi.org/10.1038/s41592-020-0912-y
43. Liu X, Salokas K, Weldatsadik RG *et al.* Combined proximity labeling and affinity purification-mass spectrometry workflow for mapping and visualizing protein interaction networks. *Nat Protoc* 2020;15:3182–211. https://doi.org/10.1038/s41596-020-0365-x
44. Teo G, Liu G, Zhang J *et al.* SAINTexpress: improvements and additional features in Significance Analysis of INTeractome software. *J Proteomics* 2014;100:37–43. https://doi.org/10.1016/j.jprot.2013.10.023
45. Mellacheruvu D, Wright Z, Couzens AL *et al.* The CRAPome: a contaminant repository for affinity purification-mass spectrometry data. *Nat Methods* 2013;10:730–6. https://doi.org/10.1038/nmeth.2557
46. von Mering C, Huynen M, Jaeggi D *et al.* STRING: a database of predicted functional associations between proteins. *Nucleic Acids Res* 2003;31:258–61. https://doi.org/10.1093/nar/gkg034
47. Shannon P, Markiel A, Ozier O *et al.* Cytoscape: a software environment for integrated models of biomolecular interaction networks. *Genome Res.* 2003;13:2498–504. https://doi.org/10.1101/gr.1239303
48. Sinigaglia K, Cherian A, Du Q *et al.* An ADAR1 dsRBD3-PKR kinase domain interaction on dsRNA inhibits PKR activation. *Cell Rep* 2024;43:114618. https://doi.org/10.1016/j.celrep.2024.114618
49. Schindelin J, Arganda-Carreras I, Frise E *et al.* Fiji: an open-source platform for biological-image analysis. *Nat Methods* 2012;9:676–82. https://doi.org/10.1038/nmeth.2019
50. R Core Team. *R: A language and environment for statistical computing*. R Foundation for Statistical Computing, Vienna, Austria. 2021. https://www.R-project.org/
51. Posit team. RStudio: Integrated Development Environment for R. 2025. http://www.posit.co/.
52. Marchand V, Blanloeil-Oillo F, Helm M *et al.* Illumina-based RiboMethSeq approach for mapping of 2'-O-Me residues in RNA. *Nucleic Acids Res* 2016;44:e135. https://doi.org/10.1093/nar/gkw547
53. Tan MH, Li Q, Shanmugam R *et al.* Dynamic landscape and regulation of RNA editing in mammals. *Nature* 2017;550:249–54. https://doi.org/10.1038/nature24041
54. Oughtred R, Rust J, Chang C *et al.* The BioGRID database: a comprehensive biomedical resource of curated protein, genetic, and chemical interactions. *Protein Sci* 2021;30:187–200. https://doi.org/10.1002/pro.3978
55. Orchard S, Ammari M, Aranda B *et al.* The MIntAct project—IntAct as a common curation platform for 11 molecular interaction databases. *Nucleic Acids Res* 2014;42:D358–63. https://doi.org/10.1093/nar/gkt1115
56. Szklarczyk D, Kirsch R, Koutrouli M *et al.* The STRING database in 2023: protein–protein association networks and functional enrichment analyses for any sequenced genome of interest. *Nucleic Acids Res* 2023;51:D638–46. https://doi.org/10.1093/nar/gkac1000
57. Nie Y, Ding L, Kao PN *et al.* ADAR1 interacts with NF90 through double-stranded RNA and regulates NF90-mediated gene expression independently of RNA editing. *Mol Cell Biol* 2005;25:6956–63. https://doi.org/10.1128/MCB.25.16.6956-6963.2005
58. Jung S, von Thulen T, Yang I *et al.* A ribosomal RNA fragment with 2′,3′-cyclic phosphate and GTP-binding activity acts as RIG-I ligand. *Nucleic Acids Res* 2020;48:10397–412. https://doi.org/10.1093/nar/gkaa739
59. Valente L, Nishikura K. RNA binding-independent dimerization of adenosine deaminases acting on RNA and dominant negative effects of nonfunctional subunits on dimer functions. *J Biol Chem* 2007;282:16054–61. https://doi.org/10.1074/jbc.M611392200
60. Soderberg O, Gullberg M, Jarvius M *et al.* Direct observation of individual endogenous protein complexes *in situ* by proximity ligation. *Nat Methods* 2006;3:995–1000. https://doi.org/10.1038/nmeth947
61. Coller J, Wickens M. Tethered function assays: an adaptable approach to study RNA regulatory proteins. *Methods Enzymol* 2007;429:299–321.
62. Bos TJ, Nussbacher JK, Aigner S *et al.* Tethered function assays as tools to elucidate the molecular roles of RNA-binding proteins. *Adv Exp Med Biol* 2016;907:61–88.
63. Bertrand E, Chartrand P, Schaefer M *et al.* Localization of ASH1 mRNA particles in living yeast. *Mol Cell* 1998;2:437–45. https://doi.org/10.1016/S1097-2765(00)80143-4
64. Tutucci E, Livingston NM, Singer RH *et al.* Imaging mRNA *in vivo*, from birth to death. *Annu Rev Biophys* 2018;47:85–106. https://doi.org/10.1146/annurev-biophys-070317-033037
65. Lykke-Andersen J, Wagner E. Recruitment and activation of mRNA decay enzymes by two ARE-mediated decay activation domains in the proteins TTP and BRF-1. *Genes Dev* 2005;19:351–61. https://doi.org/10.1101/gad.1282305
66. Luo EC, Nathanson JL, Tan FE *et al.* Large-scale tethered function assays identify factors that regulate mRNA stability and translation. *Nat Struct Mol Biol* 2020;27:989–1000. https://doi.org/10.1038/s41594-020-0477-6
67. Fritzell K, Xu LD, Otrocka M *et al.* Sensitive ADAR editing reporter in cancer cells enables high-throughput screening of small molecule libraries. *Nucleic Acids Res* 2019;47:e22. https://doi.org/10.1093/nar/gky1228
68. Lubas M, Damgaard CK, Tomecki R *et al.* Exonuclease hDIS3L2 specifies an exosome-independent 3′-5′ degradation pathway of human cytoplasmic mRNA. *EMBO J* 2013;32:1855–68. https://doi.org/10.1038/emboj.2013.135
69. Tafforeau L, Zorbas C, Langhendries JL *et al.* The complexity of human ribosome biogenesis revealed by systematic nucleolar screening of Pre-rRNA processing factors. *Mol Cell* 2013;51:539–51. https://doi.org/10.1016/j.molcel.2013.08.011
70. Leeman-Neill RJ, Song D, Bizarro J *et al.* Noncoding mutations cause super-enhancer retargeting resulting in protein synthesis dysregulation during B cell lymphoma progression. *Nat Genet* 2023;55:2160–74. https://doi.org/10.1038/s41588-023-01561-1
71. Schillewaert S, Wacheul L, Lhomme F *et al.* The evolutionarily conserved protein Las1 is required for pre-rRNA processing at both ends of ITS2. *Mol Cell Biol* 2012;32:430–44. https://doi.org/10.1128/MCB.06019-11
72. Dragon F, Gallagher JE, Compagnone-Post PA *et al.* A large nucleolar U3 ribonucleoprotein required for 18S ribosomal RNA biogenesis. *Nature* 2002;417:967–70. https://doi.org/10.1038/nature00769
73. Osheim YN, French SL, Keck KM *et al.* Pre-18S ribosomal RNA is structurally compacted into the SSU processome prior to being cleaved from nascent transcripts in *Saccharomyces cerevisiae*. *Mol Cell* 2004;16:943–54. https://doi.org/10.1016/j.molcel.2004.11.031
74. Sharma S, Marchand V, Motorin Y *et al.* Identification of sites of 2′-O-methylation vulnerability in human ribosomal RNAs by systematic mapping. *Sci Rep* 2017;7:11490. https://doi.org/10.1038/s41598-017-09734-9
75. Birkedal U, Christensen-Dalsgaard M, Krogh N *et al.* Profiling of ribose methylations in RNA by high-throughput sequencing. *Angew Chem Int Ed* 2015;54:451–5. https://doi.org/10.1002/anie.201408362

76. Macias S, Cordiner RA, Gautier P *et al.* DGCR8 acts as an adaptor for the exosome complex to degrade double-stranded structured RNAs. *Mol Cell* 2015;60:873–85. https://doi.org/10.1016/j.molcel.2015.11.011
77. Weick EM, Puno MR, Januszyk K *et al.* Helicase-dependent RNA decay illuminated by a cryo-EM structure of a human nuclear RNA exosome-MTR4 Complex. *Cell* 2018;173:1663–77.e21. https://doi.org/10.1016/j.cell.2018.05.041
78. Staals RH, Bronkhorst AW, Schilders G *et al.* Dis3-like 1: a novel exoribonuclease associated with the human exosome. *EMBO J* 2010;29:2358–67. https://doi.org/10.1038/emboj.2010.122
79. Tomecki R, Kristiansen MS, Lykke-Andersen S *et al.* The human core exosome interacts with differentially localized processive RNases: hDIS3 and hDIS3L. *EMBO J* 2010;29:2342–57. https://doi.org/10.1038/emboj.2010.121
80. Banani SF, Lee HO, Hyman AA *et al.* Biomolecular condensates: organizers of cellular biochemistry. *Nat Rev Mol Cell Biol* 2017;18:285–98. https://doi.org/10.1038/nrm.2017.7
81. Giudice J, Jiang H. Splicing regulation through biomolecular condensates and membraneless organelles. *Nat Rev Mol Cell Biol* 2024;25:683–700. https://doi.org/10.1038/s41580-024-00739-7
82. Sabari BR, Dall'Agnese A, Young RA. Biomolecular condensates in the nucleus. *Trends Biochem Sci* 2020;45:961–77. https://doi.org/10.1016/j.tibs.2020.06.007
83. Lafontaine DLJ, Riback JA, Bascetin R *et al.* The nucleolus as a multiphase liquid condensate. *Nat Rev Mol Cell Biol* 2021;22:165–82. https://doi.org/10.1038/s41580-020-0272-6
84. Ng SK, Weissbach R, Ronson GE *et al.* Proteins that contain a functional Z-DNA-binding domain localize to cytoplasmic stress granules. *Nucleic Acids Res* 2013;41:9786–99. https://doi.org/10.1093/nar/gkt750
85. Weissbach R, Scadden ADJ. Tudor-SN and ADAR1 are components of cytoplasmic stress granules. *RNA* 2012;18:462–71. https://doi.org/10.1261/rna.027656.111
86. Burke JM, Lester ET, Tauber D *et al.* RNase L promotes the formation of unique ribonucleoprotein granules distinct from stress granules. *J Biol Chem* 2020;295:1426–38. https://doi.org/10.1074/jbc.RA119.011638
87. Corbet GA, Burke JM, Bublitz GR *et al.* dsRNA-induced condensation of antiviral proteins modulates PKR activity. *Proc Natl Acad Sci USA* 2022;119:e2204235119. https://doi.org/10.1073/pnas.2204235119
88. Fox AH, Nakagawa S, Hirose T *et al.* Paraspeckles: where long noncoding RNA meets phase separation. *Trends Biochem Sci* 2018;43:124–35. https://doi.org/10.1016/j.tibs.2017.12.001
89. Uhl L, Aziba A, Lobbert S *et al.* MYC binding to nascent RNA suppresses innate immune signaling by R-loop-derived RNA–DNA hybrids. *Cell* 2026;189:1371–88. https://doi.org/10.1016/j.cell.2025.12.019
90. Choi Y, Um B, Na Y *et al.* Time-resolved profiling of RNA binding proteins throughout the mRNA life cycle. *Mol Cell* 2024;84:1764–82. https://doi.org/10.1016/j.molcel.2024.03.012
91. Langhendries JL, Nicolas E, Doumont G *et al.* The human box C/D snoRNAs U3 and U8 are required for pre-rRNA processing and tumorigenesis. *Oncotarget* 2016;7:59519–34. https://doi.org/10.18632/oncotarget.11148
92. Song Y, Yang W, Fu Q *et al.* irCLASH reveals RNA substrates recognized by human ADARs. *Nat Struct Mol Biol* 2020;27:351–62. https://doi.org/10.1038/s41594-020-0398-4
93. Imamura K, Garland W, Schmid M *et al.* A functional connection between the Microprocessor and a variant NEXT complex. *Mol Cell* 2024;84:4158–74. https://doi.org/10.1016/j.molcel.2024.10.015
94. Barak M, Porath HT, Finkelstein G *et al.* Purifying selection of long dsRNA is the first line of defense against false activation of innate immunity. *Genome Biol* 2020;21:26. https://doi.org/10.1186/s13059-020-1937-3
95. Eckard SC, Rice GI, Fabre A *et al.* The SKIV2L RNA exosome limits activation of the RIG-I-like receptors. *Nat Immunol* 2014;15:839–45. https://doi.org/10.1038/ni.2948
96. Yang K, Dong B, Asthana A *et al.* RNA helicase SKIV2L limits antiviral defense and autoinflammation elicited by the OAS-RNase L pathway. *EMBO J* 2024;43:3876–94. https://doi.org/10.1038/s44318-024-00187-1
97. Brickner JR, Garzon JL, Cimprich KA. Walking a tightrope: the complex balancing act of R-loops in genome stability. *Mol Cell* 2022;82:2267–97. https://doi.org/10.1016/j.molcel.2022.04.014
98. Lim J, Giri PK, Kazadi D *et al.* Nuclear proximity of Mtr4 to RNA exosome restricts DNA mutational asymmetry. *Cell* 2017;169:523–37. https://doi.org/10.1016/j.cell.2017.03.043
99. Pefanis E, Wang J, Rothschild G *et al.* RNA exosome-regulated long non-coding RNA transcription controls super-enhancer activity. *Cell* 2015;161:774–89. https://doi.org/10.1016/j.cell.2015.04.034
100. Puno MR, Lima CD. Structural basis for MTR4–ZCCHC8 interactions that stimulate the MTR4 helicase in the nuclear exosome-targeting complex. *Proc Natl Acad Sci USA* 2018;115:E5506–15. https://doi.org/10.1073/pnas.1803530115
101. Domingo-Prim J, Endara-Coll M, Bonath F *et al.* EXOSC10 is required for RPA assembly and controlled DNA end resection at DNA double-strand breaks. *Nat Commun* 2019;10:2135. https://doi.org/10.1038/s41467-019-10153-9
102. Gritti I, Basso V, Rinchai D *et al.* Loss of ribonuclease DIS3 hampers genome integrity in myeloma by disrupting DNA:RNA hybrid metabolism. *EMBO J* 2022;41:e108040. https://doi.org/10.15252/embj.2021108040
103. Shiromoto Y, Sakurai M, Minakuchi M *et al.* ADAR1 RNA editing enzyme regulates R-loop formation and genome stability at telomeres in cancer cells. *Nat Commun* 2021;12:1654. https://doi.org/10.1038/s41467-021-21921-x
104. Jimeno S, Prados-Carvajal R, Fernandez-Avila MJ *et al.* ADAR-mediated RNA editing of DNA:RNA hybrids is required for DNA double strand break repair. *Nat Commun* 2021;12:5512. https://doi.org/10.1038/s41467-021-25790-2
105. Zhang B, Li Y, Zhang J *et al.* ADAR1 links R-loop homeostasis to ATR activation in replication stress response. *Nucleic Acids Res* 2023;51:11668–87. https://doi.org/10.1093/nar/gkad839
106. Yi Z, Qu L, Tang H *et al.* Engineered circular ADAR-recruiting RNAs increase the efficiency and fidelity of RNA editing *in vitro* and *in vivo*. *Nat Biotechnol* 2022;40:946–55. https://doi.org/10.1038/s41587-021-01180-3
107. Perez-Riverol Y, Bandla C, Kundu DJ *et al.* The PRIDE database at 20 years: 2025 update. *Nucleic Acids Res* 2025;53:D543–53. https://doi.org/10.1093/nar/gkae1011

Received: January 5, 2026. **Revised:** March 27, 2026. **Accepted:** April 7, 2026